LBNL-51884

GEO-SEQ Project
Quarterly Status and Cost Report

D. Cole[1], C. A. Doughty[2], G. M. Hoversten[2], S. D. Hovorka[3], K. G. Knauss[4], A. R. Kovscek[5], D. H.-S. Law[6], M. J. Lippmann[2], L. R. Myer[2], R. L. Newmark[4], C. M. Oldenburg[2], K. Pruess[2]

[1]Oak Ridge National Lab, [2]Lawrence Berkeley National Lab,
[3]University of Texas at Austin, [4]Lawrence Livermore National Lab,
[5]Stanford University, [6]Alberta Research Council Petroleum Recovery Institute

June 1–August 31, 2002

This work was supported by the Assistant Secretary for Fossil Energy, Office of Coal and Power Systems of the U.S. Department of Energy through the National Energy Technology Laboratory under DOE Contract No. DE-AC03-76SF00098.

DISCLAIMER

GEO-SEQ Project
Quarterly Status and Cost Report
June 1–August 31, 2002

Project Overview

The purpose of the GEO-SEQ Project is to establish a public-private R&D partnership that will:

- Lower the cost of geologic sequestration by: (1) developing innovative optimization methods for sequestration technologies with collateral economic benefits, such as enhanced oil recovery (EOR), enhanced gas recovery (EGR), and enhanced coalbed methane production; and (2) understanding and optimizing trade-offs between CO_2 separation and capture costs, compression and transportation costs, and geologic sequestration alternatives.
- Lower the risk of geologic sequestration by: (1) providing the information needed to select sites for safe and effective sequestration, (2) increasing confidence in the effectiveness and safety of sequestration by identifying and demonstrating cost-effective monitoring technologies, and (3) improving performance-assessment methods to predict and verify that long-term sequestration practices are safe, effective, and do not introduce any unintended environmental impact.
- Decrease the time to implementation by: (1) pursuing early opportunities for pilot tests with our private-sector partners and (2) gaining public acceptance.

In May 2000, a project kickoff meeting was held at Ernest Orlando Lawrence Berkeley National Laboratory (Berkeley Lab) to plan the technical work to be carried out, starting with FY00 funding allocations. Since then, work has been performed on four tasks: (A) development of sequestration co-optimization methods for EOR, depleted gas reservoirs, and brine formations; (B) evaluation and demonstration of monitoring technologies for verification, optimization, and safety; (C) enhancement and comparison of computer-simulation models for predicting, assessing, and optimizing geologic sequestration in brine, oil, and gas, and coalbed methane formations; and (D) improvement of the methodology and information available for capacity assessment of sequestration sites.

This Quarter's Highlights

- A planning workshop for the Frio Brine Pilot Project was held at the University of Texas Bureau of Economic Geology (BEG), Austin, Texas, on July 8–9, 2002. Representatives of the various research groups involved in the project presented the latest research results and evaluated different monitoring techniques to be used during and after the upcoming CO_2 injection test. A time line and an implementation plan for the modeling, well testing, and monitoring activities were developed.
- Preliminary reactive transport simulations were carried out to illustrate the type of chemical and mineralogical changes that may result from injection of CO_2 into the Frio Formation.
- Scoping sensitivity studies of electrical-resistance tomography (ERT) and tiltmeter methods to monitor the Frio site during and after injection were performed. Preliminary results show that ERT methods have the potential to detect changes caused by CO_2 injection, while tiltmeter signals may approach detection limits.
- An economic-feasibility assessment of carbon sequestration with enhanced gas recovery showed that it is economic for CO_2/CH_4 volume ratios of 1.5 when the CO_2 price is less than approximately $10 per ton (i.e., it is marginally achievable for natural CO_2 sources in some parts of the U.S.).
- Analysis of recent (February 2002) samples collected at Lost Hills, California, showed that the contribution of injected CO_2 to the gas sampled decreases with time.

- An experimental plan for the flow-through column has been developed. A series of tracer injections are designed to measure the interaction of different tracers with various solid and liquid phases, representing common reservoir materials.
- Reservoir code intercomparison activities based on test problems continued. They showed an overall satisfactory agreement between simulators, increasing confidence in codes and computational results.
- After considering the revised injection plan developed during the Frio project-planning workshop (i.e., focusing on injecting CO_2 into the "C Sand" instead of the shallower "B Sand"), we carried out a new set of modeling studies for the South Liberty Field. They showed that the change does not dramatically affect the behavior of the CO_2 plume in the subsurface modeled earlier.

Papers Presented, Submitted, Accepted, or Published during This Quarter

Benson, S.M. et al., 2002, The GEO-SEQ Project: A status report. Paper to be presented at the Sixth International Conference on Greenhouse Gas Technologies (GHGT-6), Kyoto, Japan, October 1–4, 2002.

Boram, L.H., S.R. Higgins, K.G. Knauss, and C.M. Eggleston, 2002, Plagioclase dissolution and carbonate growth related to CO_2 sequestration in deep aquifers: EQ3/6 modeling and laboratory experiments. Paper to be presented at the 2002 GSA Annual Meeting and Exposition, Denver, Colorado, Oct. 27–30, 2002.

Doughty, C., S.M. Benson, and K. Pruess, 2002, Capacity investigation of brine-bearing sands for geologic sequestration of CO_2. Paper to be presented at the Sixth International Conference on Greenhouse Gas Technologies (GHGT-6), Kyoto, Japan, October 1–4, 2002.

Gunter, W.D. and D.H.-S. Law, 2002, Enhanced Coalbed Methane Recovery and CO_2 Storage: Simulation Issues and Model Comparison. Paper to be presented at the International Workshop on the "Present Status and Outlook of CO_2 Sequestration in Coal Seam," Tokyo, Japan, September 5, 2002.

Holtz, M.H., 2003, Pore-scale influences on saline aquifer CO_2 sequestration. Abstract submitted to the American Association of Petroleum Geologists Annual Meeting, Salt Lake City, Utah, May 11–14, 2003.

Hovorka, S. D. and P.R. Knox, 2002, Frio Brine sequestration pilot in the Texas Gulf Coast. Paper to be presented at the Sixth International Conference on Greenhouse Gas Technologies (GHGT-6), Kyoto, Japan, October 1–4, 2002.

Hoversten, G.M., R. Gritto, T.M. Daley, E.L. Majer, and L.R. Myer, 2002, Crosswell seismic and electromagnetic monitoring of CO_2 sequestration. Paper to be presented at the Sixth International Conference on Greenhouse Gas Technologies (GHGT-6), Kyoto, Japan, October 1-4, 2002.

Jin, M., M. Delshad, D.C. McKinney, G.A. Pope, K. Sepehrnoori, C. Tilberg, and R.E. Jackson. 1994, Subsurface NAPL contamination: Partitioning Tracer Test for Detection, Estimation and Remediation Performance Assessment. In: Toxic Substances in Hydrologic Sciences, Amer. Intst. of Hydrology, pp. 131-159, Minneapolis.

Johnson, J.W. et al., 2002, CO_2 floods for co-optimized EOR and sequestration: Technology development and demonstration. Paper to be presented at the Sixth International Conference on Greenhouse Gas Technologies (GHGT-6), Kyoto, Japan, October 1–4, 2002.

Johnson, J.W. and J.J. Nitao, 2002, Reactive transport modeling of geologic CO_2 sequestration at

Sleipner. Paper to be presented at the Sixth International Conference on Greenhouse Gas Technologies (GHGT-6), Kyoto, Japan, October 1–4, 2002.

Johnson, J.W., J.J. Nitao, R.L. Newmark, B.A. Kirkendall, G.J. Nimz, K.G. Knauss, and J.P. Ziagos, 2002, Geologic CO_2 sequestration: Predicting and confirming performance in oil reservoirs and saline aquifers. Paper presented at the AGU Annual Spring Meeting, Washington, D.C., May 28–31, 2002.

Johnson, J.W., J.J. Nitao, C.I. Steefe, and K. G. Knauss, 2002, Reactive transport modeling of geologic CO_2 sequestration. Paper to be presented at the 2002 GSA Annual Meeting and Exposition, Denver, Colorado, Oct. 27–30, 2002.

Knauss, K.G., J.W. Johnson, and L.H. Boram, 2002, Impact of CO_2, contaminant gas, aqueous fluid, and reservoir rock interactions on the geologic sequestration of CO_2. Paper to be presented at the 2002 GSA Annual Meeting and Exposition, Denver, Colorado, Oct. 27–30, 2002.

Knox, P.R., C. Doughty, and S.D. Hovorka, 2003, Impacts of buoyancy and pressure gradient on field-scale geological sequestration of CO_2 in saline formations. Abstract submitted to the American Association of Petroleum Geologists Annual meeting, Salt Lake City, Utah, May 11–14, 2003.

Kovscek, A. R., 2002, Screening criteria for CO2 storage in oil reservoirs. Petroleum Science and Technology, 20 (7/8), 841-866.

Law, D.H.-S, L.H.G. van der Meer, and W.D. Gunter, 2002, Comparison of numerical simulators for greenhouse gas storage in coalbeds, Part II: Flue gas injection. Paper to be presented at the Sixth International Conference on Greenhouse Gas Technologies (GHGT-6), Kyoto, Japan, October 1–4, 2002.

Law, D.H.-S, L.H.G. van der Meer, P. Sammon, L. Pekot, and W.D. Gunter, 2002, New development on coalbed methane simulators for enhanced coalbed methane recovery processes. Geological Society of America Annual Meeting, Denver, Colorado, October 27–30, 2002 (abstract originally submitted to the 4th Annual CBM Conference, Calgary, Alberta, Canada, October 23–25, 2002).

Myer, L.R., G.M. Hoversten, and C.A. Doughty, 2002, Sensitivity and cost of monitoring geologic sequestration using geophysics. Paper to be presented at the Sixth International Conference on Greenhouse Gas Technologies (GHGT-6), Kyoto, Japan, October 1–4, 2002.

Newmark, R., A. Ramirez, and W. Daily, 2002, Monitoring carbon dioxide sequestration using electrical resistance tomography (ERT): a minimally invasive method. Paper to be presented at the Sixth International Conference on Greenhouse Gas Technologies (GHGT-6), Kyoto, Japan, October 1–4, 2002.

Oldenburg, C.M., 2002, Carbon dioxide as cushion gas for natural gas storage. Paper submitted to Energy & Fuels.

Oldenburg, C.M., D.H.-S. Law, Y. Le Gallo, and S.P. 2002, White, Mixing of CO_2 and CH_4 in gas reservoirs: Code comparison studies. Paper to be presented at the Sixth International Conference on Greenhouse Gas Technologies (GHGT-6), Kyoto, Japan, October 1–4, 2002.

Oldenburg, C.M., S.H. Stevens, and S.M. Benson, 2002, Economic feasibility of carbon sequestration with enhanced gas recovery (CSEGR). Paper to be presented at the Sixth International Conference on Greenhouse Gas Technologies (GHGT-6), Kyoto, Japan, October 1-4, 2002.

Pruess, K., A. Bielinski, J. Ennis-King, R. Fabriol, Y. Le Gallo, J. García, K. Jessen, T. Kovscek, D. H.-S. Law, P. Lichtner, C. Oldenburg, R. Pawar, J. Rutqvist, C. Steefel, B. Travis, C.F. Tsang, S. White, and T. Xu, 2002, Code intercomparison builds confidence in numerical models for geologic disposal of CO_2. Paper to be presented at the Sixth International Conference on Greenhouse Gas Technologies (GHGT-6), Kyoto, Japan, October 1–4, 2002.

Rau, G.H., K. Caldeira, and K. Knauss, 2002, A geochemical solution to the atmospheric CO_2 problem? Paper to be presented at the 2002 GSA Annual Meeting and Exposition, Denver, Colorado, Oct. 27–30, 2002.

Task Summaries

Task A: Develop Sequestration Co-Optimization Methods

Subtask A-1: Co-Optimization of Carbon Sequestration, EOR, and EGR from Oil Reservoirs

Goals

To assess the possibilities for co-optimization of CO_2 sequestration and EOR, and to develop techniques for selecting the optimum gas composition for injection. Results will lay the groundwork necessary for rapidly evaluating the performance of candidate sequestration sites, as well as monitoring the performance of CO_2 EOR.

Previous Main Achievements

- Screening criteria for selection of oil reservoirs that would co-optimize EOR and maximize CO_2 storage in a reservoir have been generated.
- An engineering approach to increase CO_2 storage during EOR has been developed.

Accomplishments This Quarter

- The development of a method to select rationally subsets of models that consider realistic reservoir flow scenarios, while spanning the spectrum of uncertainty, is near completion.

Progress This Quarter

Previously, we developed a synthetic, 3-D, geostatistical model of an oil reservoir. It is based upon the permeability characteristics of an actual field and includes a realistic multicomponent chemical description of reservoir fluids. The model incorporates uncertainty, in that various realizations constrained by measured data can be obtained. From among the large number of possible realizations, we need to select a much smaller number that encompasses our uncertainty regarding the true geology. It is upon this subset that computationally expensive flow simulations are conducted. We have (almost) developed a systematic and efficient method to select a subset of reservoir models that span the range of possible flow behavior. Thus, we probe effectively the uncertainty inherent in prediction.

Yuandong Wang, a postdoctoral researcher, was hired. He will work on techniques to maximize oil recovery and CO_2 storage, as well as efficient techniques for incorporating geologic uncertainty into reservoir simulation predictions.

Work Next Quarter

We will continue to consider, through reservoir simulation, various reservoir-development scenarios, so that we can better understand techniques that maximize the simultaneous production of oil and storage of CO_2. These scenarios will be evaluated using the reservoir models chosen above. We are examining (in order): water-alternating-gas (WAG) drive mode, CO_2 injection early in production life versus late in reservoir life, CO_2 injection following water flooding, and the stripping of CO_2 from a mixture of CO_2 and N_2 that simulates an incompletely separated combustion gas.

Additionally, it is quite clear from our work to date, as well as from oil industry experience, that control of the mobility of CO_2 relative to oil is key to improving displacement and storage efficiency. An experimental effort examining the ability of aqueous foams (soap and brine) to trap CO_2 within the pore space of rock will begin. The *in situ* distribution of CO_2 will be imaged using x-ray computed tomography.

Subtask A-2: Feasibility Assessment of Carbon Sequestration with Enhanced Gas Recovery (CSEGR) in Depleted Gas Reservoirs

Goals

To assess the feasibility of injecting CO_2 into depleted natural gas reservoirs for sequestering carbon and enhancing methane (CH_4) recovery. Investigation will include assessments of (1) CO_2 and CH_4 flow and transport processes, (2) injection strategies that retard mixing, (3) novel approaches to inhibit mixing, and (4) identification of candidate sites for a pilot study.

Previous Main Achievements

- On the basis of numerical-simulation studies, the proof-of-concept for CO_2 storage with enhanced gas recovery (CSEGR) has been demonstrated.
- Initial feasibility was assessed through numerical simulation of CO_2 injection into a model system, based on the Rio Vista gas field in California.
- The numerical-simulation capability supporting this assessment is being improved through enhancement of the TOUGH2-EOS7C code.

Accomplishments This Quarter

- We continued the economic-feasibility assessment study of CSEGR.
- We finalized a number of conference and journal papers.

Progress This Quarter

Curt Oldenburg worked with Scott Stevens (ARI) to carry out an economic-feasibility assessment of CSEGR. Using the Rio Vista Gas Field in California as the test case, they compiled incremental costs, capital costs, and incremental revenues to form a spreadsheet model capable of assessing the economics of CSEGR at Rio Vista. A simple pattern of injectors and producers was assumed, with injection rates based on the 680 MW gas-fired power plant in Antioch, California.

The physical behavior of the injection most relevant to economic feasibility is the CO_2/CH_4 volume ratio, a measure of the volume of CO_2 that must be injected per incremental volume of CH_4 produced. This ratio is greater than unity because of the large compressibility of CO_2 and because CO_2 is highly soluble in water. The results are presented in **Figure 1**. As shown in the figure, CSEGR is economic for CO_2/CH_4 volume ratios of 1.5 when the CO_2 price is less than approximately \$10/ton. This is marginally achievable for natural CO_2 sources in some parts of the country. However, the cost of CO_2 captured from power plants is much larger (\$50/ton), so subsidy will be required for CSEGR to be profitable if CO_2 from power plants is to be used under current conditions.

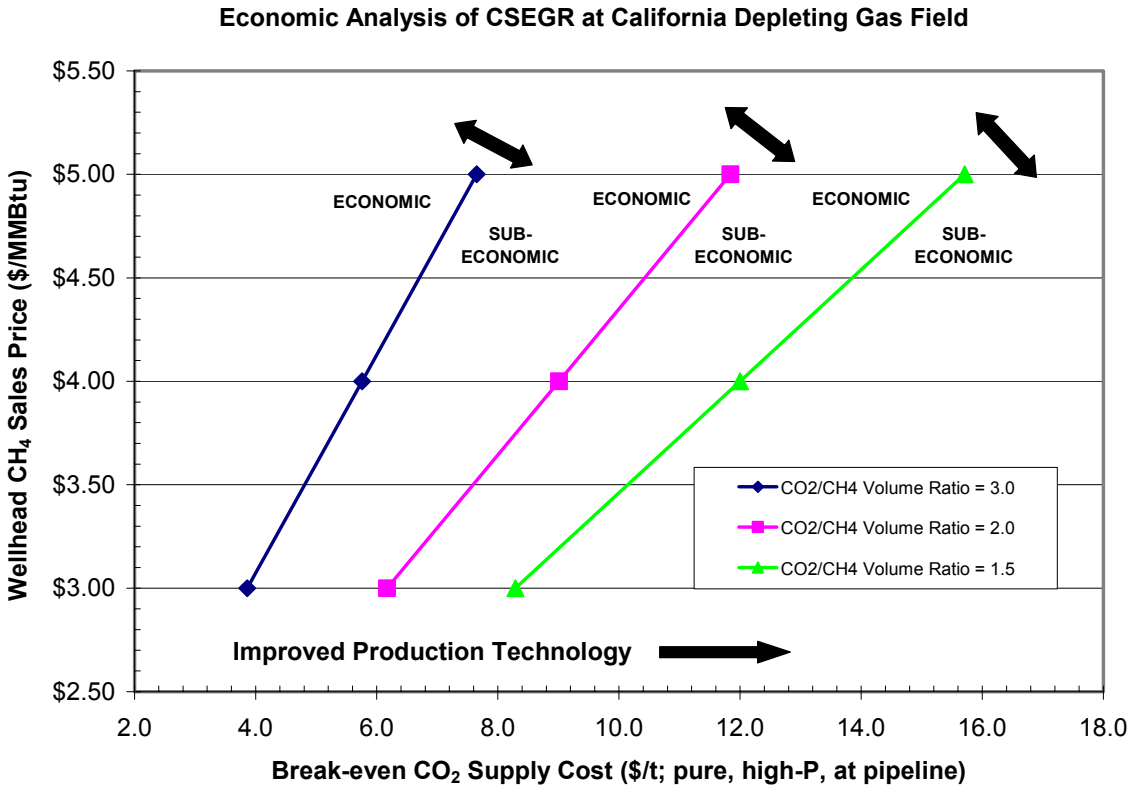

Figure 1. Results of sensitivity analysis showing actual break-even CO_2 supply costs (no subsidy) for various CH_4 prices

Work Next Quarter

- Complete economic-feasibility-assessment work for additional regions in the U.S.
- Write paper on the comparison of DGM and ADM to include variation in Knudsen diffusion coefficient as a function of permeability.

Subtask A-3: Evaluation of the Impact of CO_2 Aqueous Fluid and Reservoir Rock Interactions on the Geologic Sequestration of CO_2, with Special Emphasis on Economic Implications.

Goals

To evaluate the impact on geologic sequestration of injecting an impure CO_2 waste stream into the storage formation. By reducing the costs of the front-end processes, the overall costs of sequestration could be dramatically lowered. One approach is to sequester non-pure CO_2 waste streams that are less expensive or require less energy than separating pure CO_2 from the flue gas.

Previous Main Achievements

- Potential reaction products have been determined based upon reaction-progress chemical thermodynamic/kinetic calculations for typical sandstone and carbonate reservoirs into which an impure CO_2 waste stream is injected.

Accomplishments This Quarter

- Reactive-transport (open system) chemical kinetic simulations were run, using the reactive-transport simulator CRUNCH (Steefel, 2001). These new simulations were made in support of planning for the Frio Brine Pilot Project in Texas (Task E).

Confirmatory reactive-transport experiments, intended to lend credibility to the model calculations and simulations done to date and planned for the future, were designed using this same simulator. This past quarter, we completed reactive-transport simulations for a plug-flow reactor (PFR) run to be made using the Frio Formation core material recently acquired from the University of Texas BEG.

- The Frio Formation core samples were subcored for geophysical measurements, and the remaining material was disaggregated for use in the PFR.

Progress This Quarter

The process of evaluating the impact of waste stream CO_2, as well as contaminants (e.g., SO_2, NO_2, and H_2S), on injectivity and sequestration performance continued.

Representative core samples of both the Frio Formation “C” sand and the overlying shale caprock were obtained during the meeting held at BEG in early July (see Task E). The samples were taken from Well Felix Jackson #62, drilled by Sun Oil Company in 1977 and located within the Oyster Bayou field in Chambers County, Texas. The sampled sand was from the interval 8,184.7– 8,185 ft, while the shale was from the interval 8159.5–8159.7 ft. Several one-inch subcores were taken from each core sample by dry coring. These will be used primarily for geophysical lab measurements. The remaining shale material was gently crushed and dry-sieved to $20 \geq x \geq 40$ mesh. The resulting grains were simply aggregates of the much-smaller-sized shale particles themselves, but the aggregated grains are now a coarse sand size ideal for insertion into the PFR. The remaining sand material was simply disaggregated and not sieved. The sand grains were poorly cemented and of a medium-to-fine size already (see **Figure 2**).

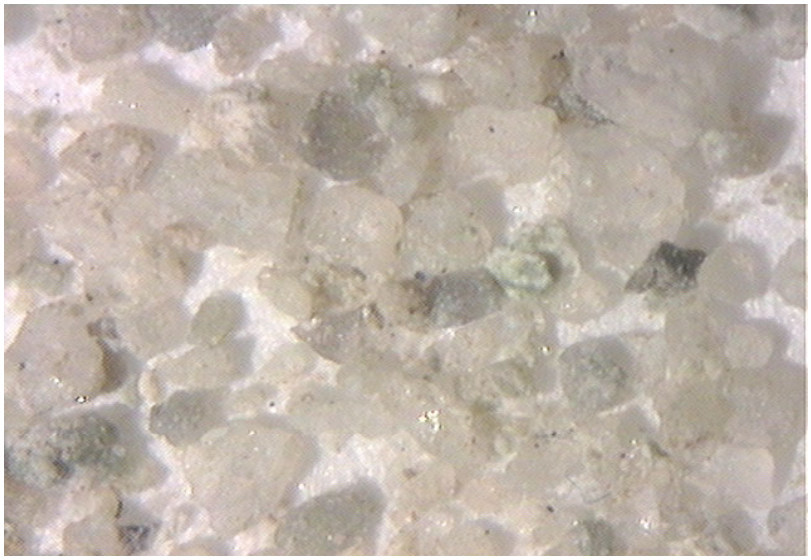

Figure 2. Sand grains from one of the Felix Jackson #62 samples (see text). The greenish grain near the center is ~300 microns long

The preliminary reactive-transport simulations were done using CRUNCH. The goal was to try to anticipate chemical and mineralogical changes that we might expect to see in a one-year Frio Brine Pilot Project (Task E), consisting of a two-month injection period followed by 10 months of post-injection observation. Because our interests are primarily in chemistry, we set the problem up

as a very simple 1-D simulation, which approximates a single streamline between an injection well, and an observation or production well. We further simplified transport by only considering flow of a single (liquid) phase, because in the field we will be acquiring primarily liquid aqueous samples (including dissolved gases) from observation well(s).

In recent TOUGH2 simulations of CO_2 injection into the "C" sand (250 T/d, 60 days), Chris Doughty (Berkeley Lab) found that after five days, the liquid-phase linear velocities were up to 1.8 x 10^{-5} m/sec. We used this velocity as a constant liquid velocity in our simulation for the 60 days of injection and then arbitrarily dropped the rate to one-tenth that value for the post injection period. We assumed a downhole temperature of 55°C and the same total pressure (150b CO_2) as in the TOUGH2 simulation. This results in a CO_2 fugacity of 84.3 b. We also used the same sand porosity of 29%.

In our simulation, the mineralogy of the Frio Formation "C" sand was assumed to be that found at a stratigraphically equivalent depth in the Merisol WDW No. 319 well, located in Harris County, Texas. The modal abundances and compositions were determined using XRD in a report provided by Dan Collins (Sandia Tech). The starting mineralogy consisted of the appropriate mix of quartz, K-feldspar, plagioclase (represented as a mixture of albite and anorthite end-members), pyrite, muscovite (as a proxy for illite), kaolinite, clinochlore (as the magnesium end-member chlorite) and calcite as the cement mineral. Because the formation fluid becomes very acidic (pH 3.3) near the injection well, we used full kinetic-rate laws for each mineral, accounting for acid catalysis. The chemical elements comprising the model formation fluid were based on compositions for Frio Formation waters taken from the nearby Harris County well GNI WDW-169 included Ca, Mg, Ba, Sr, Na, Cl, S, Fe, C, Al, Si, and H. Preliminary equilibrium modeling required to speciate the model water at run initialization suggested that possible secondary minerals included barite, chalcedony, dawsonite, magnesite, siderite, and strontianite. These minerals could precipitate, as well as any of the primary minerals, and kinetic-rate laws also governed precipitation.

As examples of our preliminary results, we show in **Figures 3 and 4** the breakthrough curves (i.e., the output from nodes within the modeled domain) for elements of potential interest at various distances along the 135 m flow path between the proposed injection and observation wells at South Liberty. Note that the observation well shows modest concentration increases in K and Si throughout the simulation, even though the other chemical results suggest that the impact of the injected CO_2 has not yet reached the observation well. This is because the starting formation fluid is slightly under saturated with respect to K-feldspar solubility, and thus this mineral dissolves slowly throughout the simulation. This process is reasonable chemically, given that in the Frio Formation natural diagenesis results in K-feldspar decomposition, as it is converted to illite, and as the NaCl brine causes albitization of the K-feldspar (i.e., the exchange of Na for K).

The primary impact of injecting CO_2 is to drive the pH down, buffered by the calcite cement, although the cement is completely consumed near the wellbore and the pH drops to nearly the value fixed by CO fugacity. The low pH destabilizes many of the primary minerals, and they dissolve, increasing the fluid concentrations of Ca (from calcite and anorthite), Mg (from clinochlore), K (from K-feldspar) and Si (from all of the silicates). Although not plotted (owing to the scale), Al also increases in concentration, due to dissolution of aluminosilicates, primarily K-feldspar.

The particular flow rates and time periods used in this simulation would suggest that the chemical signal in the aqueous phase progresses between 50 and 90 m from the injection well, never quite making it to the observation well. Of course, this calculation needs to be repeated using a simulator that more explicitly couples flow and chemistry, e.g., NUFT-C or TOUGHREACT.

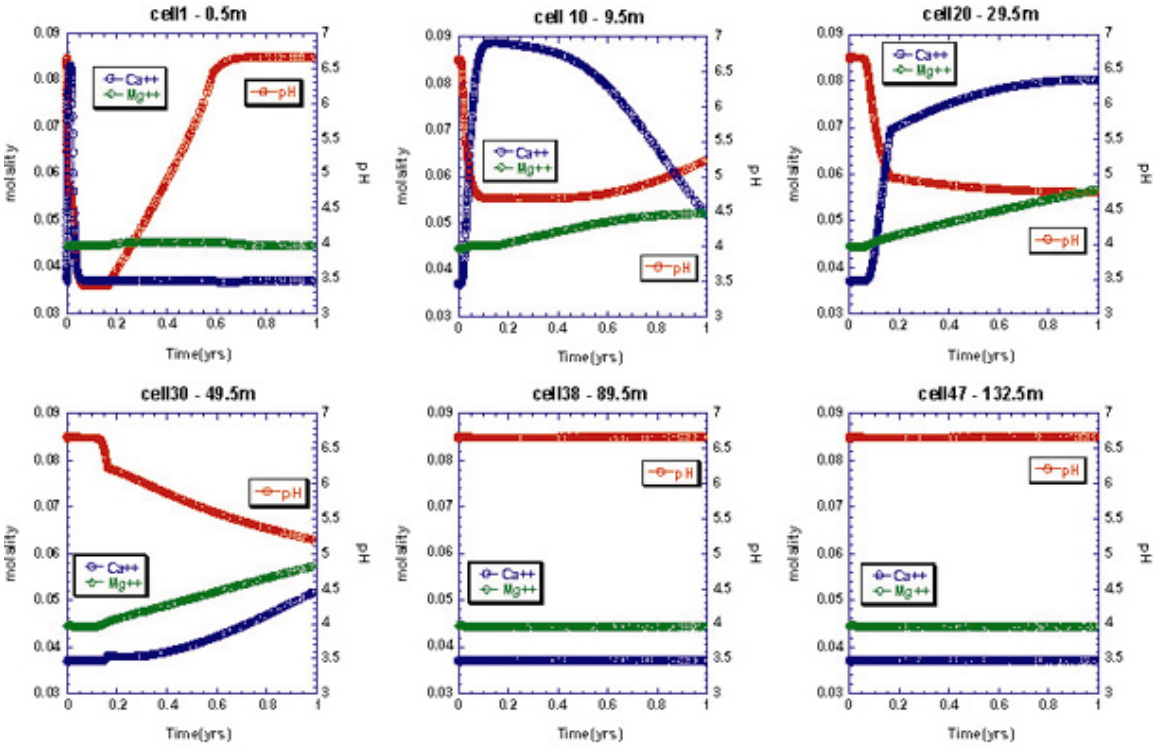

Figure 3. Breakthrough curves at several distances from the injection well

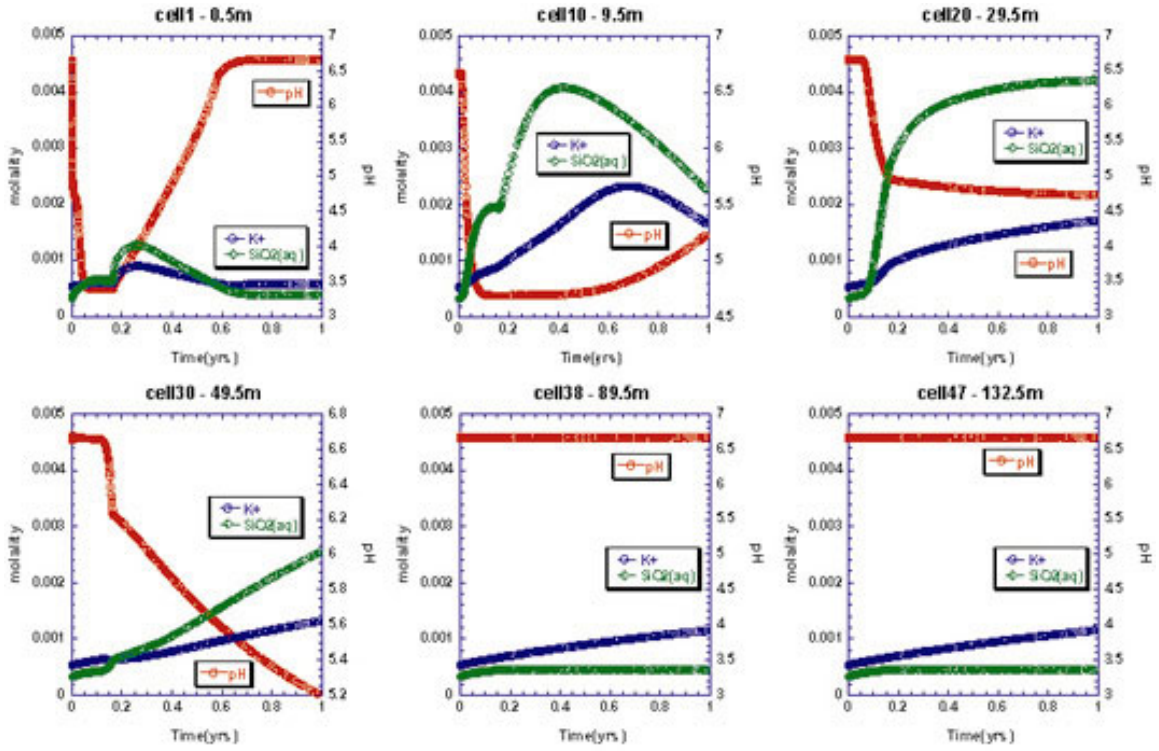

Figure 4. Breakthrough curves at several distances from the injection well

Also of interest is the simulated formation of several carbonate minerals along the flow path, in locations in space and time primarily dictated by the fluid pH. **Figure 5** shows that dawsonite and

magnesite are predicted to form. Although not plotted because of the much larger concentration scale, calcite is also predicted to form at pH values comparable to those occurring where magnesite is predicted to grow (i.e., about one pH unit higher than where dawsonite is stable). Although some of the carbonate predicted to grow simply represents mobilized carbonate cement, the bulk of it represents CO_2 carbon being sequestered by mineral trapping. In terms of total mass, however, over this short time period the mass of carbon sequestered by solubility in the aqueous phase dwarfs that sequestered by carbonate mineral precipitation.

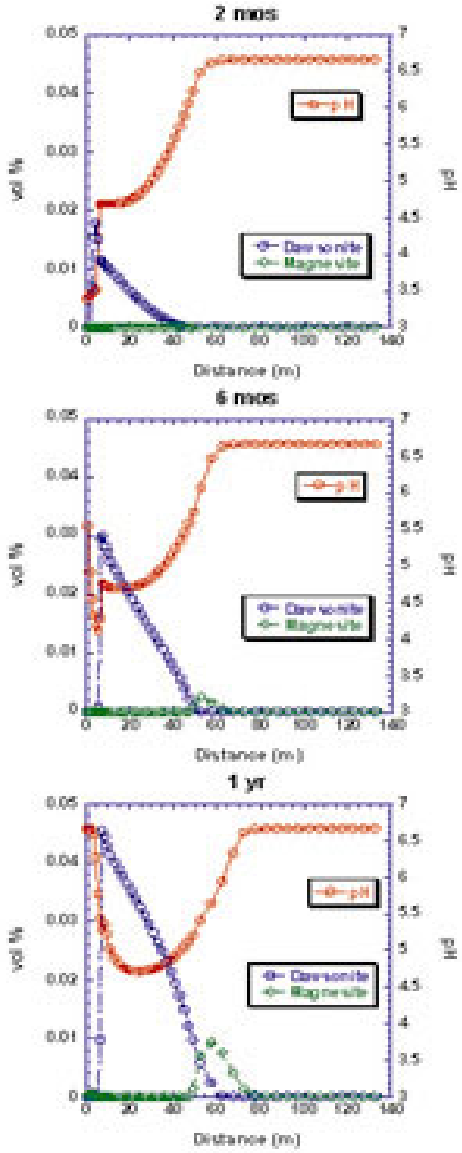

Figure 5. Mineral distribution away from the injection well at various times

These simulations, although hydrologically simplistic, illustrate the types of chemical and mineralogical changes that we might expect from CO_2 injection in a Frio Formation-type setting. If more completely coupled simulations confirm that the aqueous-phase chemical signal for the current test design (250 T/d, 60 days) may not reach the proposed observation well, such confirmation would argue for drilling a new well, probably an injection well, closer to the currently proposed observation well.

Work Next Quarter

We will continue investigating the impact of other contaminants (SO_2, H_2S, NO_2, etc.) in the CO_2 waste stream. Our attention will become more focused on doing work that may help in designing and conducting the Frio Brine Pilot Project (Task E). For example, we plan to redo the calculations shown here using a radial, rather than a linear, flow-velocity field, to more closely resemble the TOUGH2 modeling being done by Chris Doughty (Berkeley Lab). We will also conduct simulations similar to those described here, but with longer injection times, longer post injection time periods, and in the presence of contaminant gases (e.g., H_2S, SO_2) in the waste stream.

Task B: Evaluate and Demonstrate Monitoring Technologies

Subtask B-1: Sensitivity Modeling and Optimization of Geophysical Monitoring Technologies

Goals

To (1) demonstrate methodologies for, and carry out an assessment of, the effectiveness of candidate geophysical monitoring techniques; (2) provide and demonstrate a methodology for designing an optimum monitoring system; and (3) provide and demonstrate methodologies for interpreting geophysical and reservoir data to obtain high-resolution reservoir images. The Chevron CO_2 pilot at Lost Hills, California, is being used as an initial test case for developing these methodologies.

Previous Main Achievements

- A methodology for site-specific selection of monitoring technologies was established and demonstrated.

Accomplishments This Quarter

- Modeling studies based on well logs from the Liberty Field in south Texas showed that before CO_2 injection, seismic reflection from shale-sand interfaces decreases in amplitude with increasing depth. As CO_2 is injected at shallow depth, there is a sharp decrease in reflectivity.
- The studies also indicated that even if a CO_2 wedge were seismically detected because of geometric effects, interpretation of the reflection for fluid properties would be difficult until the horizontal extent of the CO_2 zone exceeds one seismic Fresnel zone.

Progress This Quarter

A study was carried out to evaluate the sensitivity of surface seismic techniques for monitoring of CO_2 sequestration. Two issues were addressed: (1) the contrast in seismic properties produced by injection of CO_2 and (2) spatial resolution.

Contrast in Seismic Properties

The contrast in seismic properties was characterized by calculating changes in the reflectivity, or magnitude, of the reflection of a normally incident wave at the boundary between two thick layers.

Reflectivity, R, is given by:

$$R = \frac{I_2 - I_1}{I_2 + I_1} = \frac{\rho_2 V_2 - \rho_1 V_1}{\rho_2 V_2 + \rho_1 V_1}$$

where I I is the impedance of the layer, V is the velocity, and ρ is density. This equation shows that reflections are generated at the boundary between different lithologies, and they can also be

generated by fluid contrasts. Injection of CO_2 will potentially alter the reflectivity of pre-existing lithologic boundaries or create new reflections.

Calculations were carried out to study changes of reflectivity as a function of depth for CO_2 in brine formations. It is assumed that fluid pressures are given by the normal hydrostatic gradient for water. A thermal gradient of 10ºC per 1,000 ft. is assumed. It is also assumed that CO_2 is injected only into the sands with a porosity of 20%. In **Figure 6**, reflectivity is calculated as a function of depth for a boundary between shale and sandstone. In **Figure 7,** the boundary is between sand containing CO_2 and sand containing brine.

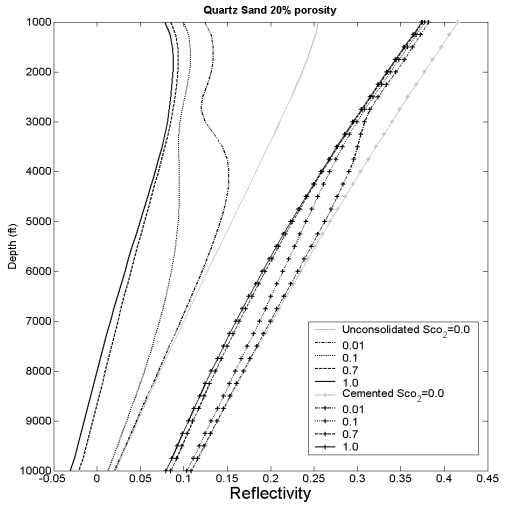

Figure 6. Reflectivity of a shale-sand boundary where sand has 20% porosity and S_{CO2} refers to the CO_2 saturation in the sand sand.
layer. Shale properties are taken from averaged well log values, and sand properties are calculated using Gassmann's equation for fluid substitution into a dry frame whose modulus is based on sands for Liberty Field, south Texas. Solid curves are for unconsolidated sand and the curves with symbols are for cemented sandstone.

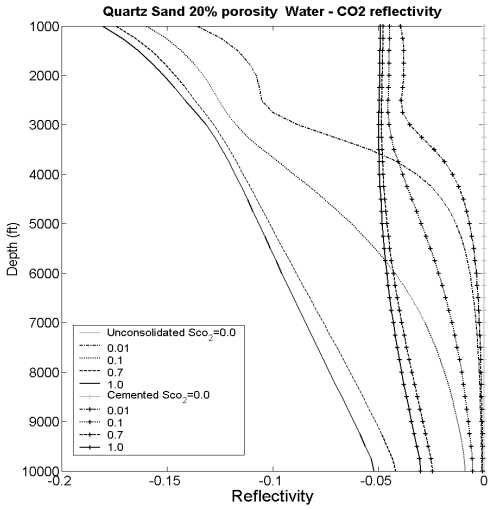

Figure 7. Reflectivity of a boundary between 20% sand containing CO_2 and brine saturated

S_{CO2} is the CO_2 saturation. See Figure 6 for other parameters.

In both cases, calculations were carried out for consolidated sandstone with clay cement and unconsolidated sand. Bulk densities were calculated using a saturation-based mixing law. The density of brine as a function of pressure and temperature was obtained from work of Batzle and Wang (1992). The density of brine increases with increasing pressure and decreases with increasing temperature. For *in situ* conditions of this study, the thermal-density decrease is essentially offset by the pressure-density increase. Bulk and shear moduli of the dry sand frame were calculated using the approach of Dvorkin and Nur (1996). The bulk moduli of CO_2 and brine were derived from results of Magee and Howley (1994) and Batzle and Wang (1992), respectively. Wood's equation (Batzle and Wang, 1992) is used for the effective bulk modulus of pore fluid mixtures, and Gassmann's equation (Gassmann, 1951) is used for the effective bulk modulus of the sand containing the fluid.

Shale density and shale velocity as a function of depth were obtained from well logs considered typical of a Texas Gulf Coast geologic setting. The V_p for water-saturated shale varied from 1,750 m/sec at 1,000 ft to almost 3,000 m/sec at 10,000 ft. The V_p for water-saturated consolidated sand

was about 3,800 m/sec at 1,000 ft, increasing by about 1% over the entire depth range. The V_p for water-saturated unconsolidated sand increased from about 2,620 m/sec at 1,000 ft to about 3,050 m/sec at 10,000 ft. These velocities are also considered typical of Texas Gulf Coast sediments. Differences between the unconsolidated and consolidated sand velocities reflect the differences in rock-frame rigidity and the influence of increasing overburden pressure on this rigidity.
For conditions assumed in the study, **Figure 7** shows that the reflection from the shale-sand interface decreases in amplitude with increasing depth before CO_2 injection. As CO_2 is injected, at shallow depth, reflectivity decreases dramatically. This decrease is primarily caused by the reduction in sand velocity, which approaches that of the shale. Only a small amount of CO_2 (0.01 saturation) is required to cause the velocity reduction, which is consistent with the known effect of "gas-like" fluids. This effect is not observed below 4,000 ft, where the seismic properties of CO_2 are more "liquid-like." For unconsolidated sand, at higher levels of saturation, reflectivity goes to zero and then begins to increase in the negative direction. This means that the amplitude of the reflection would go to zero and then start to increase with a change in phase. For consolidated sand, the effect of injected CO_2 is to reduce reflectivity at all depths. The effects of saturation are less for the consolidated sand because of the rigidity of the rock frame. If the shale velocity were higher than the sand velocity, the effects of saturation shown in **Figure 7** would be reversed. That is, at shallow depths, a small amount of CO_2 would increase the amplitude of the reflection from the shale boundary.

In **Figure 8,** the reflectivity for the brine-saturated condition is zero. Introduction of CO_2 results in a reflection, the amplitude of which is close to that generated when CO_2 is injected at a shale boundary. The reflectivity is always negative because the impedance of the sand with CO_2 is always less than that of sand with brine.

Spatial Resolution

The size of the region containing CO_2 must be sufficient to generate an interpretable signal at the surface. To begin to put bounds on the minimum size for detectability, investigators performed seismic simulations using a model in which a wedge of CO_2 is placed in a brine-saturated, unconsolidated sand layer (**Figure 8**). The CO_2 saturation in the wedge was assumed to be 50%. The wedge is a rough approximation of the shape of the plume formed by CO_2 injected into (or leaking into) the base of the sand layer. The thickness of the sand varied from 5 m to 100 m. The width of the wedge was based on the size of the first Fresnel zone. The amplitude of the reflection from an object with a size on the order of our Fresnel zone or smaller will be affected by the size of the object, in addition to the impedance contrast. Volumes of CO_2 of this size may be detected but not easily characterized.

Results of calculations for a sand layer at 2,000 m depth are given in **Figures 9** and **10**. At this depth, the shale has V_p=2,700 m/sec and a density of 2,160 kg/m^3. The sand has V_p=3,050 m/sec and a density of 2,260 m/sec; the CO_2 wedge has V_p=2,530 m/sec and a density of 2,245 kg/m^3. The seismic-wave center frequency was 30 Hz, which is consistent with observations of the frequency content of surface seismic in Texas Gulf Coast sediments. For these conditions, the first Fresnel zone diameter is about 320 m. Calculations were therefore carried out for wedge widths of 160 m, 320 m, and 480 m. An acoustic finite- difference simulation was carried out using an "exploding reflector," which produces the equivalent of a zero-offset stacked section. A Kirchoff time migration was run on the results to produce the plots shown in **Figures 9 and 10.**

The model with a 5 m thick sand layer generated no discernable reflection. This is understandable, since the layer thickness was on the order of 5% of the seismic wavelength. Results for the 10 m thick layers are shown in **Figure 9**. The sand layer generates a reflection, but no reflection is observed in the center of the CO_2 wedge. At 2,000 m depth, for the conditions assumed in this model, the impedance difference between the shale and the sand containing CO_2 is almost zero. **Figure 10** shows results for the 30 m thick layer. In this case, the CO_2 wedge is imaged, where the reflections are generated at the interface between the brine-saturated sand and the sand containing CO_2. The brine-saturated sand beneath the CO_2 wedge has sufficient thickness to generate a reflection.

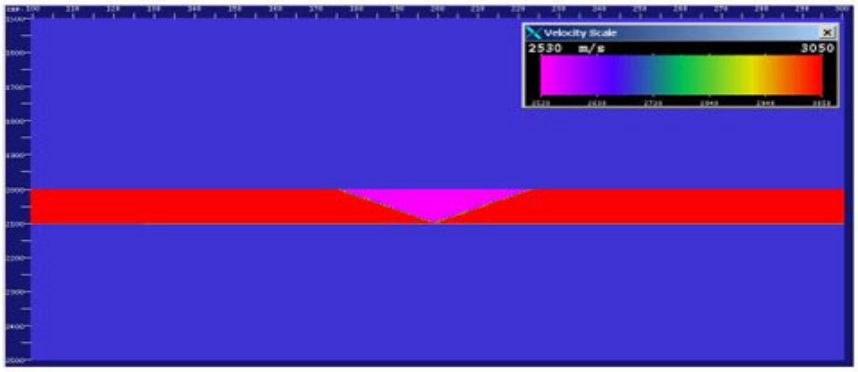

Figure 8. Velocity model for the seismic calculations, showing a wedge containing CO_2 in a sand layer

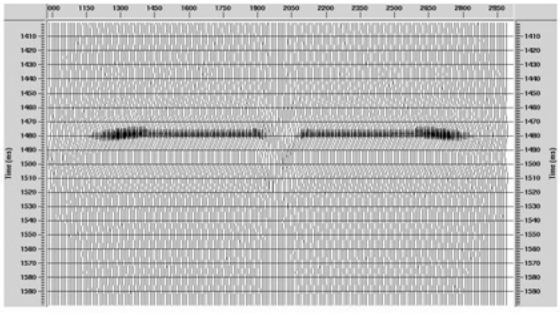

Figure 9. Reflection from a 10 m thick layer containing a 160 m wide wedge

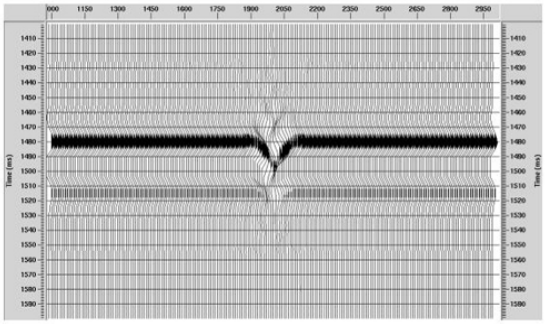

Figure 10. Reflection from a 30 m thick layer containing a 160 m wide wedge

For these models, the width of the wedge was less than a Fresnel zone, and the layer thickness was on the order of less than the layer tuning thickness. Even though the CO_2 wedge is detected, interpretation of the reflection for fluid properties would be difficult because of geometric effects. A uniform CO_2 saturation and a sharp interface between CO_2 and brine are also somewhat unrealistic.

The amount of CO_2 in a cone with diameter equal to the wedge width was calculated to put the size of seismically detectable volumes in the context of a sequestration project. For this study, the smallest wedge that could be imaged was 160 m wide. At 2,000 m depth, a cone of this diameter, 30 m high, would contain about 20,000 t of CO_2, or somewhat less than the CO_2 production in one day for a 1,000 MW coal-fired power plant. A cone large enough to prevent contamination of reflections by geometrical effects would have a diameter of 480 m and thickness of 100 m. Such a cone would contain about 17 days of CO_2 production.

References

Betzel, M. and Wang, Z., 1992, Seismic properties of pore fluids, Geophysics, 57, 1396-1408.

Dvorkin, J. and Nur, A., 1996, Elasticity of high-porosity sandstones: Theory for two North Sea data sets, Geophysics, 61, 1363-1370.

Gassmann, F., 1951, Elasticity of porous media: Uber die Elastizitat poroser Medien: Vierteljahrsschrift der Naturforschenden Gesselschaft in Zurich, Heft 1.

Magee, J. W. and Howley, J. A., 1994, A predictive model for the thermophysical properties of carbon dioxide rich mixtures, Research Report RR-136, Gas Processors Association, Tulsa, OK.

Work Next Quarter

Laboratory measurements of streaming potentials (SP) generated by CO_2 injection into brine-saturated sandstone will be made, in support of continued numerical modeling of the SP response for the upcoming Frio Brine Pilot Project CO_2 injection test (Task E).

Subtask B-2: Field Data Acquisition for CO_2 Monitoring Using Geophysical Methods

Goals

To demonstrate (through field testing) the applicability of single-well, crosswell and surface-to-borehole seismic, crosswell electromagnetic (EM), and electrical-resistance tomography (ERT) methods for subsurface imaging of CO_2.

Previous Main Achievements

- The first test of the joint application of crosswell seismic and crosswell electromagnetic measurements for CO_2 monitoring was completed.

Accomplishments This Quarter

- Performed scoping studies of sensitivity of ERT and tiltmeter methods to detect and monitor CO_2 injection as part of the Frio Brine Pilot Project.
- Refined design for upcoming time-lapse ERT survey in Chevron's Vacuum Field, where CO_2 injection is underway.

Progress This Quarter

Work focused on the Frio Brine Pilot Project (Task E). Both ERT and tiltmeter scoping studies were carried out to determine the sensitivity of these methods to the proposed CO_2 injection scenarios.

Electrical-Resistance Tomography

Using site characterization input, a forward model was constructed. Existing wells were assumed to be available for imaging, which resulted in an asymmetric pattern of nine wells (**Figure 11**). Carbon dioxide injection was simulated to occur at 1,828 m depth as a change in resistivity. Two targets shapes were considered, both of which with a modest contrast in resistivity: (1) a slab-like block of 0.5 ohm-m in a region of background resistivity of 1 ohm-m, and (2) a narrow, fingerlike anomaly migrating from the injection well, but not intersecting the monitoring well.

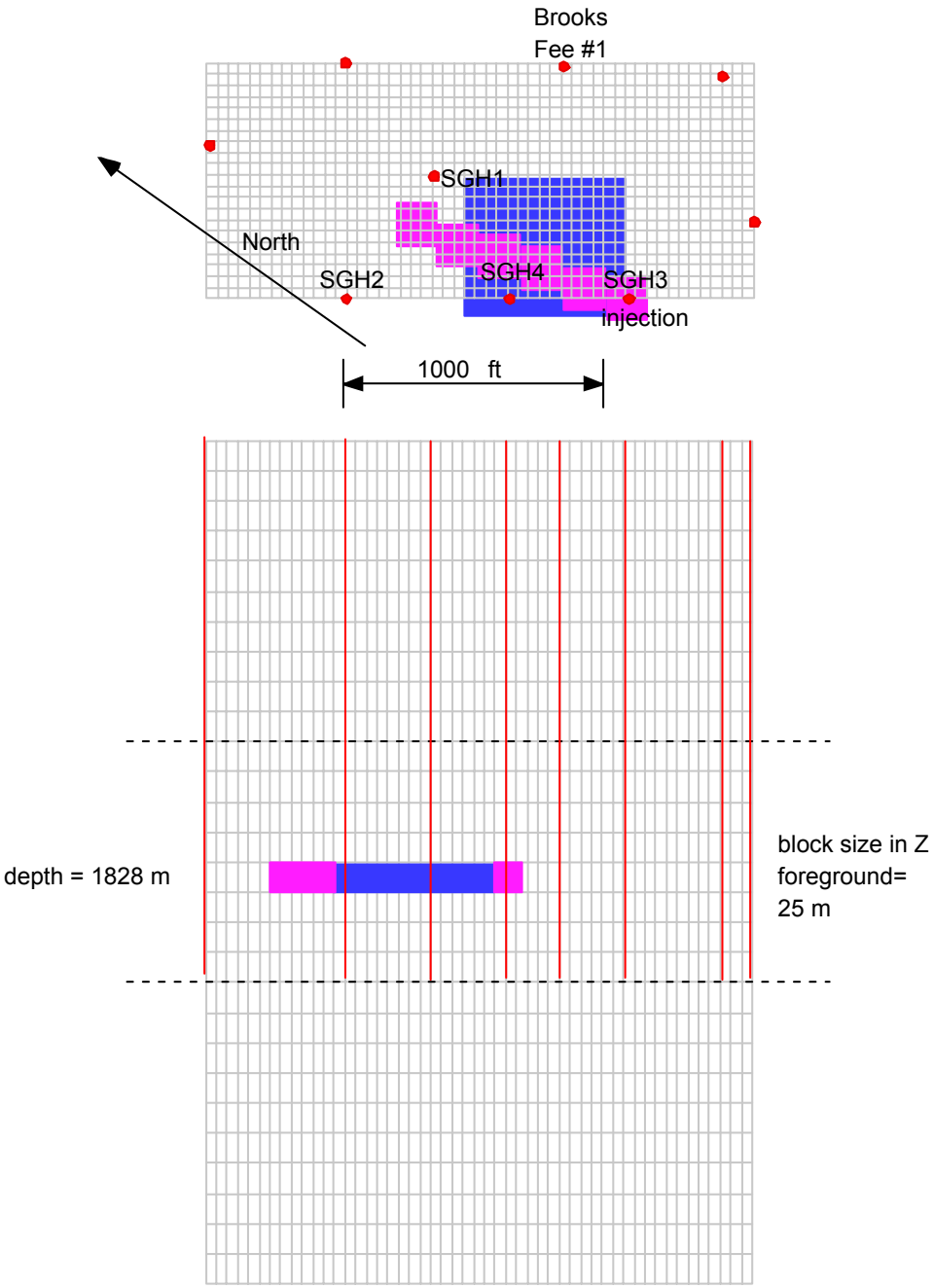

Figure 11. Forward model used to determine sensitivity of ERT methods

The current project plan calls for relatively small amounts of CO_2 to be injected. This is expected to result in a similarly small to moderate change in the reservoir as a target for detection and monitoring. Forward models confirm a small difference resulting from a moderate resistivity change **(Figure 12).**

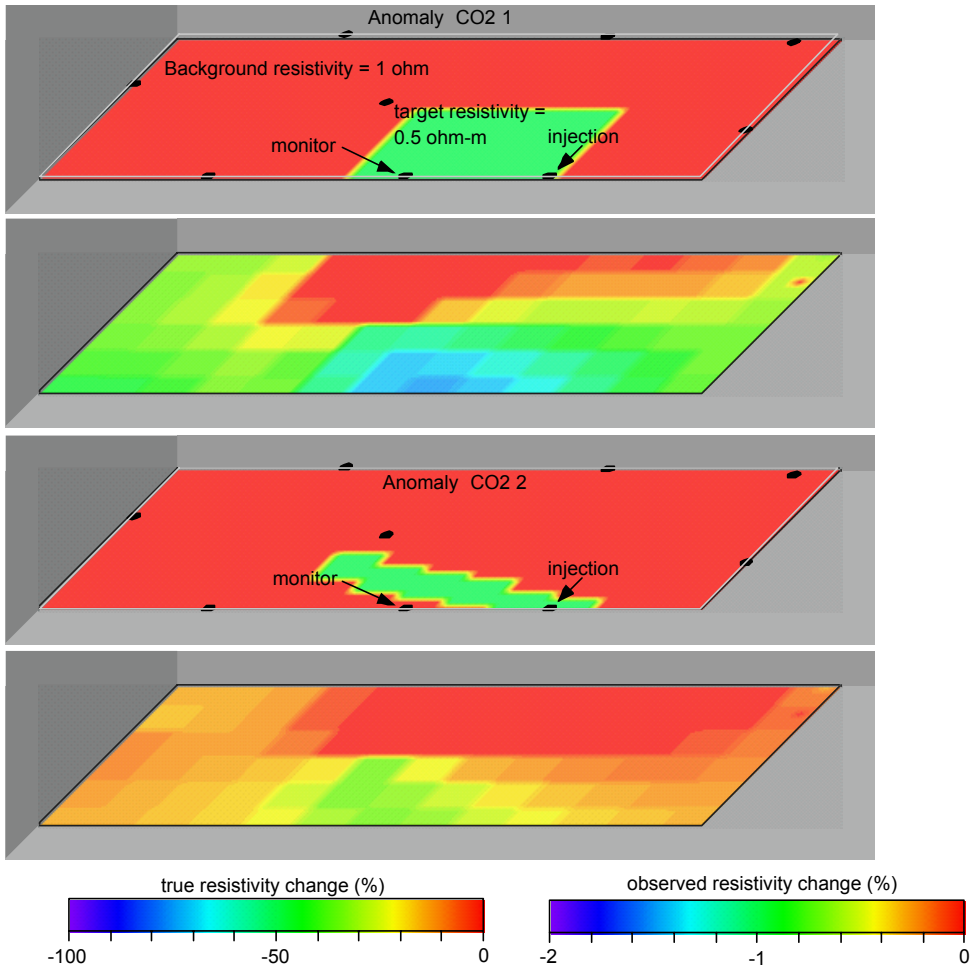

Figure 12. True and observed resistivity changes

By assessing the relative signal strength expected, we can develop an optimal field survey design for the project. Overall, the low signal strength places strong constraints on the data collection protocol.

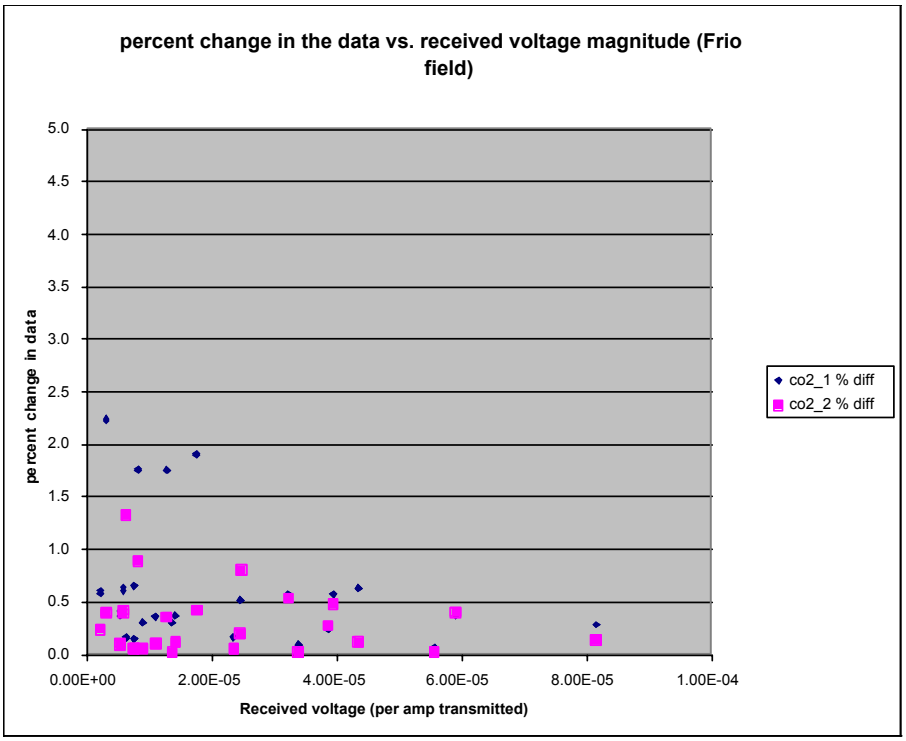

Figure 13. Frio field simulation. Percent change in the resistivity versus received voltage.

In **Figure 13**, the signal strength is shown for the two targets. In these simulations, differences are below 3%. Common signal strength for casing surveys is in the millivolt range, which is off the scale shown. However, this does not directly apply to field surveys. The plot shows received voltage per amp transmitted. Typical injection currents range from 1 to 10 amps. Injection currents in this range increase the received voltage by a factor of ten, thus bringing the simulated data into the range of practice.

Increasing the transmit power is possible, especially for a manual acquisition. This will further increase the received voltage. Field results have shown that data can be obtained with high fidelity (repeatability and reciprocity within a few percent). Thus, there is potential to design a field survey to monitor the changes resulting from CO_2 injection. A key issue involves increasing transmit power to boost signal strength. It would also be preferable to increase the volume of CO_2 injected, which would increase target size and contrast.

Tiltmeters

A scoping study to determine the potential for tiltmeter surveys to detect and monitor the movement of CO_2 at the South Liberty site was carried out. In this initial study, the source is modeled as a finite rectangular opening mode (normal displacement only) dislocation (or crack) inflated under internal pressure. The dislocation represents the fault-bounded block of the B sand as a whole. Dimensions roughly correspond to the main zone of CO_2 infiltration in the Berkeley Lab model at 100 days (dip = 15 degrees).

The crack was inflated under uniform pore pressure estimated from the pore-pressure increase at 100 days in the Berkeley Lab model. Peak pressure change is about 0.7 MPa (7 bars), and a rough estimate gives a mean of 0.6 MPa from the distribution. Opening of the dislocation, which drives the tilt calculation, is estimated from the pressure **(Figure 14).**

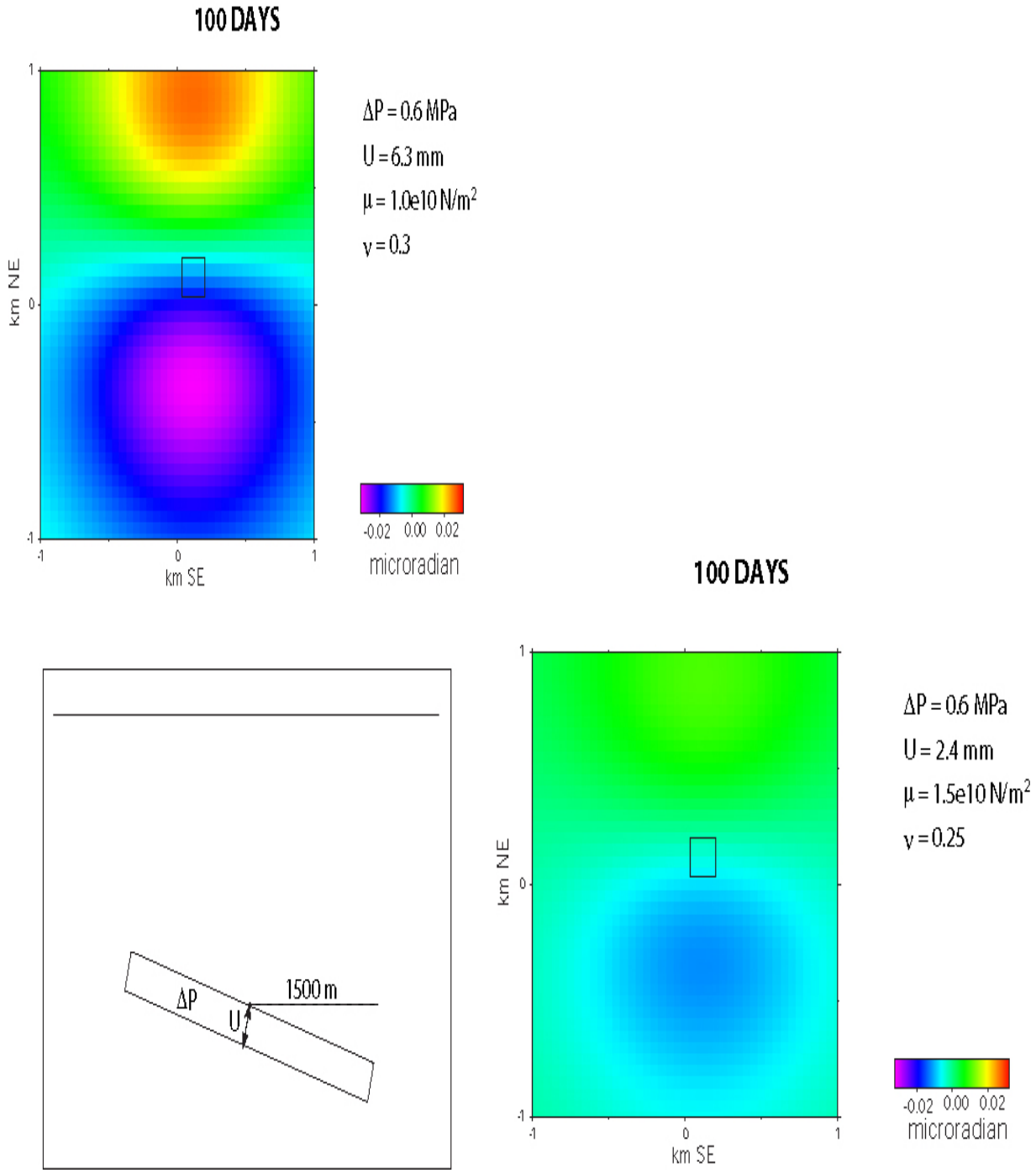

Figure 14. Details of the tiltmeter scoping study (see text)

Given that the source dimensions are about 10 times less than the source depth, the shape of the source (e.g., rectangle versus ellipse) is immaterial, at least for these scoping calculations. Some sources of uncertainty include the uncertainty in the actual elastic moduli for the site formation components; these have been estimated using different generic values for similar sedimentary rock. Noise threshold of tiltmeters is generally a few nano-radians.

For one bounding target calculation, we obtained signals of a few tens of nano-radians, which should be easily detectable at the scale of the problem. For the other, the results are marginal,

with signals approaching the limits of detection. Based on these results, a more refined simulation is being constructed to assess the potential of tiltmeters as monitors for the injection.

Samples of the Frio Formation

Representative core samples of both the Frio "Sand C" and the overlying shale caprock were collected during the early July meeting at BEG (see Subtask A-3). They will be used primarily for geophysical laboratory measurements.

Work Next Quarter

A time-lapse ERT survey will be obtained in Chevron's Vacuum Field in September. Field data will be processed and interpreted. This will be the first opportunity to detect changes associated with CO_2 injection in the field. Refined models will be run to assess the sensitivity of tiltmeters for detecting changes that result from the proposed injection of CO_2 into the Frio formation (as part of the Frio Brine Pilot Project; Task E).

Subtask B-3: Application of Natural and Introduced Tracers for Optimizing Value-Added Sequestration Technologies

Goals

To provide methods that utilize the power of natural and introduced tracers to decipher the fate and transport of CO_2 injected into the subsurface. The resulting data will be used to calibrate and validate predictive models utilized for (1) estimating CO_2 residence time, reservoir storage capacity, and storage mechanisms; (2) testing injection scenarios for process optimization; and (3) assessing the potential leakage of CO_2 from the reservoir.

Previous Main Achievements

- Laboratory isotopic-partitioning experiments and mass-balance isotopic-reaction calculations have been done to assess carbon- and oxygen-isotope changes (focused on the influence of sorption) as CO_2 reacts with potential reservoir phases.

Accomplishments This Quarter

- Gas compositions have been determined for wells sampled on 2/14/02 at Lost Hills, California, and indicate a much smaller contribution of injection CO_2 compared to the previous sampling on 11/20/01.
- Model calculations were performed to estimate the gaseous and aqueous diffusivities of perfluorocarbons tracers (PFTs) and SF_6 as a function of temperature and pressure.
- Construction and pressure testing have been completed on the dynamic flow system.

Progress This Quarter

Gas Chemistry and Stable Isotopes

Gas compositions (CO_2, C_1-C_6, N_2, O_2) have been measured for samples obtained from Lost Hills, California, on 2/14/02, during an extensive period of water injection that started in mid-November 2001. Isotope compositions were also measured in the CO_2 injectate, and CO_2 and CH_4 were separated from the production gases. Gas chemistries are plotted together with results we had obtained previously from earlier samplings on CO_2-CH_4-ΣC_2-C_6 ternaries shown in **Figure 15**. Clearly, the contribution by injectate CO_2 becomes far less pronounced over time, starting from our earliest post-injection samplings (12/6/00; 1/4/01). In fact, three of the wells, 11-8D, 12-8D, and 11-7B, exhibit gas compositions very similar to those for wells sampled prior to the initiation of the CO_2 injection test (9/19/00), which we presume represents the "baseline" reservoir chemistry. The caveat here, however, is that this part of the Lost Hills reservoir had been undergoing water injection as far back as 1/7/00, some eight months prior to the CO_2 test. Thus, the gas and isotope

chemistry of reservoir gas will never be known for this area because of the long history of perturbation.

We can get some approximate sense of the shifts in gas chemistry over a time frame of a few months by comparing chemistries from Well 11-9J sampled on 9/7/01, 11/20/01, and 2/14/02. The first and last of these sample times occurred at the end of water-injection episodes, whereas the intermediate sample date fell just a few days after CO_2 injection was stopped. The gas chemistry is clearly more "reservoir-like" during water injections, particularly for the 9/7/01 sample, which was associated with a longer-duration, higher-capacity injection compared to 2/14/02. Note that in the figure, this 2/14/02 sample has a gas chemistry intermediate to the 9/7/01 and 11/20/01 samples. The infrequency of our sampling has undoubtedly led to other missed examples of this type of shorter-term fluctuation, in both chemical and isotopic compositions.

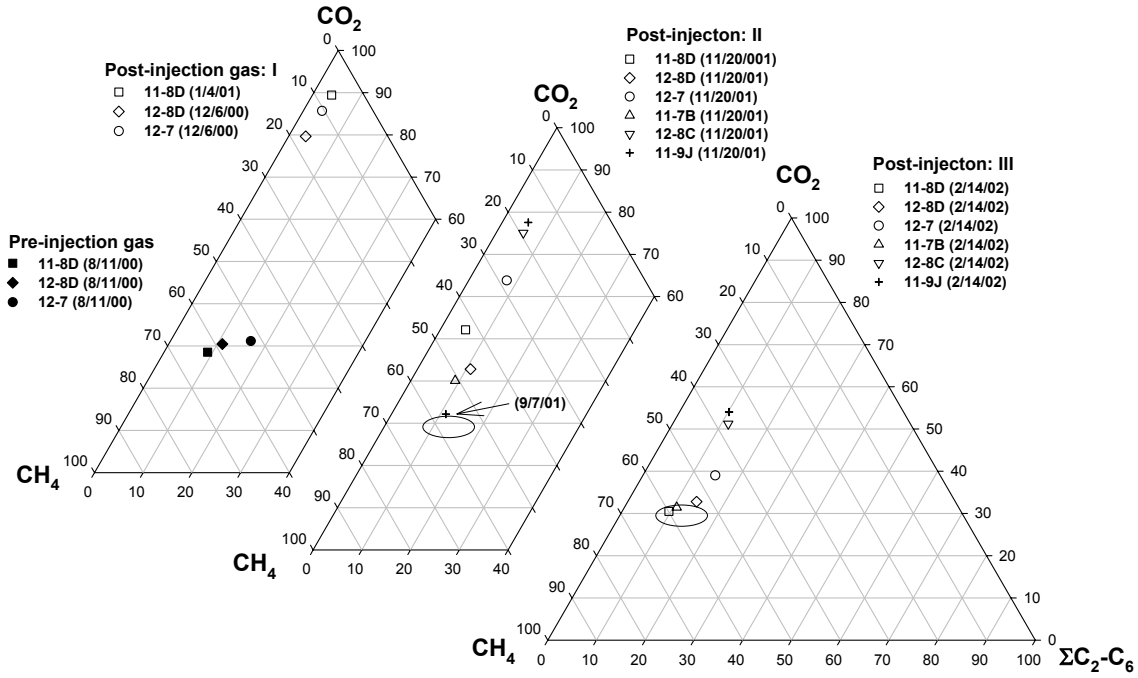

Figure 15. Gas compositions of samples obtained from the injection system at Lost Hills, California

The carbon isotope compositions of CO_2 are plotted as a function of time in **Figure 16**. It appears that isotopic values determined for samples obtained during intervals of water injection are more enriched in ^{13}C than samples obtained during or just after CO_2 injection. As mentioned above, the earliest gas samples taken prior to any CO_2 injection may not represent pristine "reservoir" gas, but do at least represent what the reservoir may have looked like prior to perturbation by CO_2. Note that first CO_2 injection interval lasted longer (111 days) and was of a higher capacity than later CO_2 injections. This might explain why the CO_2 sampled just after this first interval is nearly pure CO_2 and has carbon isotope values essentially identical to the CO_2 injectate.

It is not clear at this point what role water plays in causing shifts in gas and isotope chemistry. As a non-carbon diluent it has no affect on gas and isotope chemistry but as a separate phase it undoubtedly acts as a piston, influencing the flow and extent of mixing between existing gas and CO_2 injectate. This is further complicated by the fact that the duration and capacities of separate injections of water and CO_2 have varied over time. Another issue is the question of which of the wells were used during a particular injection test. Analyses from the next set of samples (obtained

6/20/02, with analyses in progress) will possibly provide more insight into the subsurface mixing processes

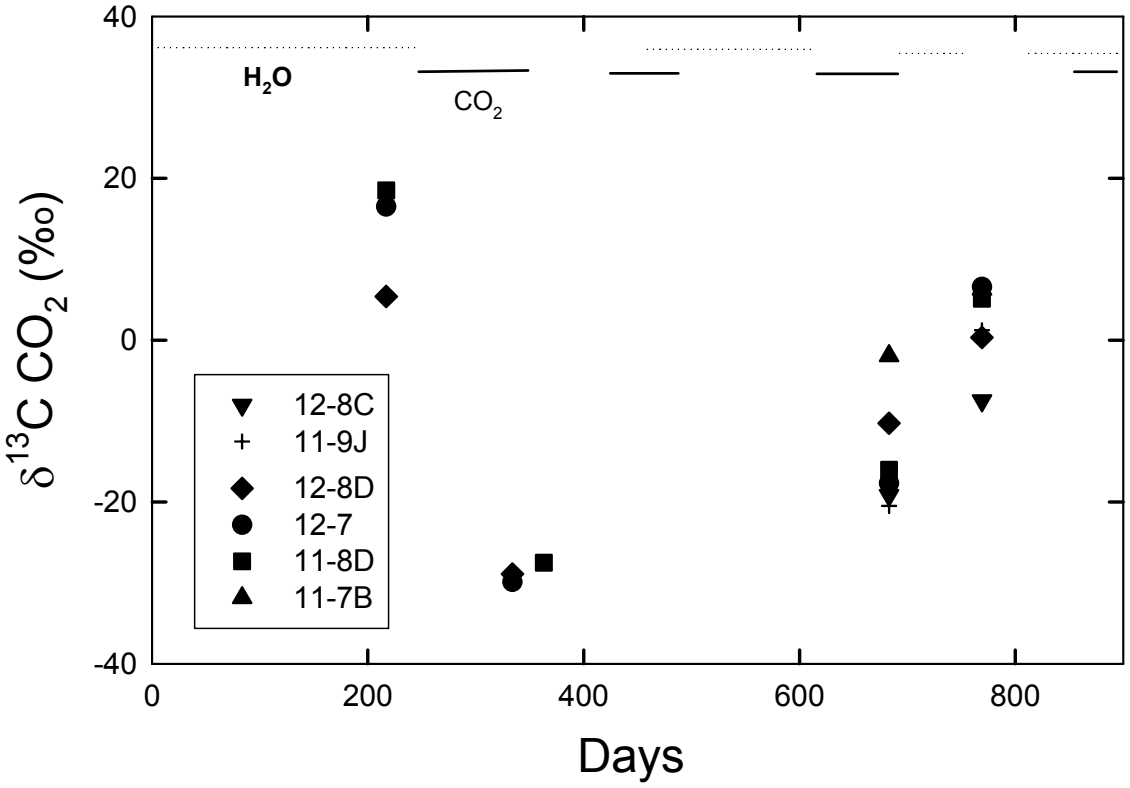

Figure 16. Plot of CO_2 carbon isotope values determined for "reservoir" samples (taken August 18, 2000 prior to CO_2 injection; 224 days after initial water injection), and CO_2 separated from samples obtained from various wells in the Lost Hills, CA system. Also shown are the intervals when either water or CO_2 were being injected (top of figure).

Applied Gas Tracer Studies

In interpreting results of injection experiments involving multiple perfluorocarbon tracers (PFTs), investigators rely upon differential responses of each tracer to specific mass-transfer processes, including matrix diffusion, sorption, and partitioning. For multi-tracer experiments in which tracer separation is used to quantify mass-transfer processes, it is necessary to quantify the differences in behavior for each tracer as they interact with various phases in the reservoir. The processes of interest for the laboratory gas-tracer experiments will include gaseous and aqueous diffusion into stagnant pore spaces, sorption onto solid phases, partitioning into brine phases, and partitioning into hydrocarbon phases. If diffusion into stagnant pores is a significant process operating in a reservoir, this will be recognized by a separation in tracer breakthrough curves for tracers with different diffusion coefficients. Therefore, we have modeled the values of gaseous and aqueous diffusion coefficients in air and water for SF_6 and PFTs, using the methods of Wilke and Lee (1955) and the Hyduck and Laudie (1974), respectively.

Figure 17 depicts plots of diffusivity in air for SF_6 and PTCH as a function of temperature and pressure, representing the extremes in response for the tracers being evaluated. Curves for all other tracers fall between those shown here. The dependency on molecular weight is apparent in the plots, with the much lighter SF_6 having the highest diffusivity.

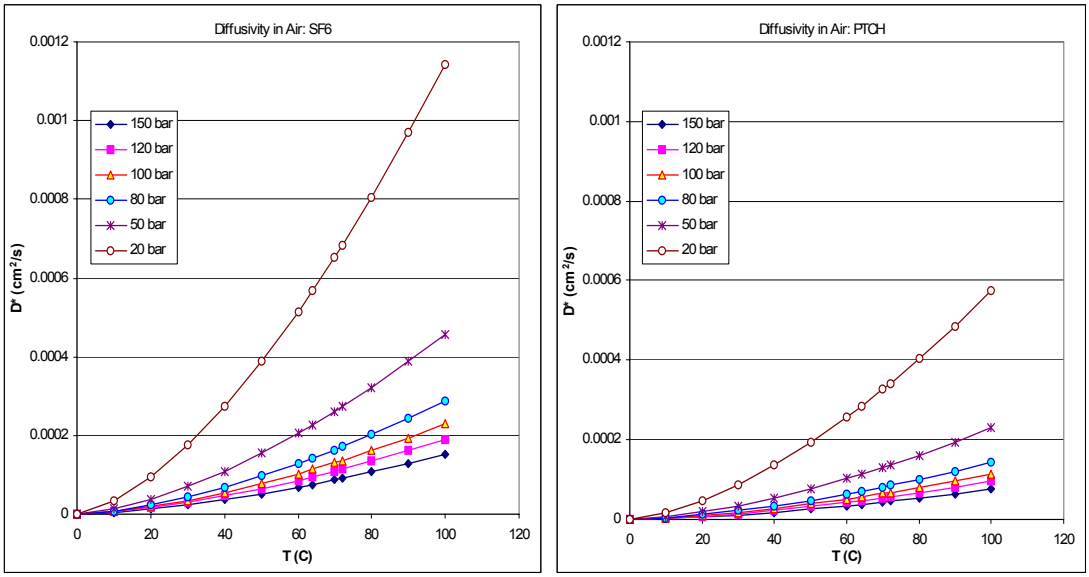

Figure 17. Diffusivity of SF_6 and PTCH as a function of temperature and pressure

Figure 18 shows diffusitivity in air as a function of temperature at 150 bars pressure. Although the differences are reduced at the temperatures likely to be encountered in the Frio Formation, there is still a factor of two difference in diffusitivity at T=64°C and P=150 bars. The difference between the diffusitivities of helium and neon is less than this, but a separation of those tracers was used by Sanford et al. (1998) to demonstrate matrix diffusion into clay and shale. Consequently, SF_6 and PTCH will likely undergo chromatographic separation during transport if stagnant pore waters are encountered. Based on the solubilities of perfluoromethyl-cyclohexane (PMCH) and perfluorodimethyl-cyclohexane (PDCH) (1.285 and 1.283 mmol/L at 20°C, respectively), the partitioning into aqueous phase is likely to be small. What partitioning there is will be influenced by the diffusitivity in water, since the speed at which molecules move away from the air-water interface will govern the concentration gradient at that location. **Figure 19** shows a plot of diffusitivity as a function of temperature for the PFTs.

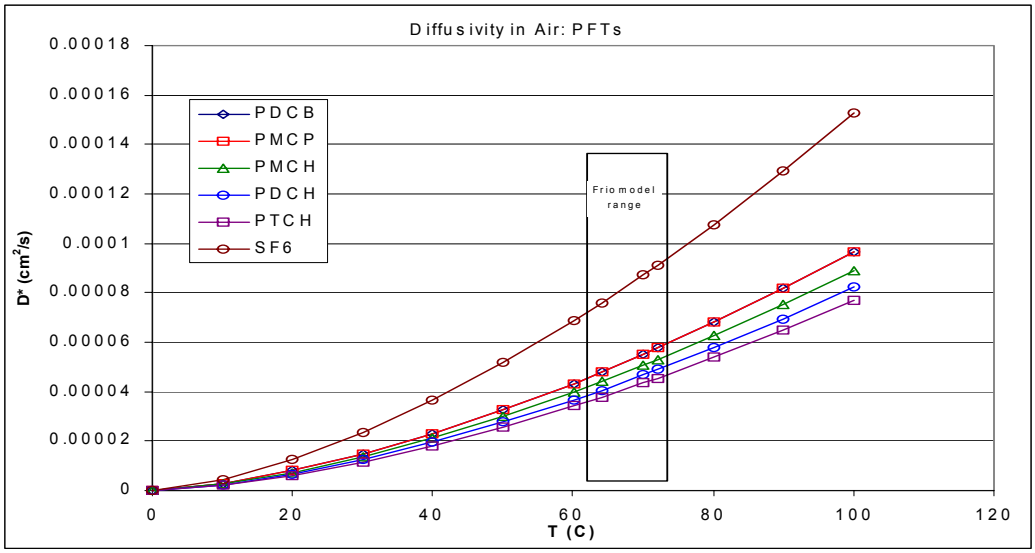

Figure 18. Diffusivity in air as a function of temperature at 150 bars pressure. The approximate temperature range anticipated in the Frio Formation is indicated.

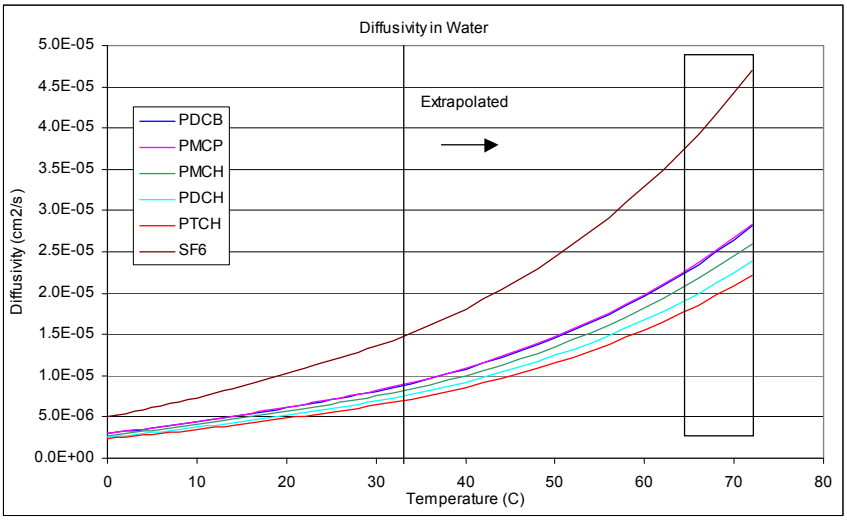

Figure 19. Diffusivity in water as a function of temperature. The box indicates the approximate range for the Frio Formation.

Thus, very low solubility of these gases is likely to cause them to act conservatively with respect to the brines of the Frio Formation. However, this will be determined by the column studies designed for this subtask.

Laboratory Flow-Through Column Experimental Plan

An experimental plan for the flow-through column, which has been completed and pressure tested, has been determined. It is based upon a sequence of tracer injections designed to measure the interaction of the individual tracers with a variety of solid and liquid phases representing common reservoir materials. Further, the differential behavior of the tracers with respect to specific transport processes is expected to enable the determination of parameters such as the presence of (and potentially the saturation of) hydrocarbons (HC's) in the reservoir. The mass-transfer mechanisms that will be tested using tracer separation techniques include diffusion into immobile pore fluids, adsorption onto the solid phase, partitioning into brines, and partitioning into hydrocarbon phases. These mechanisms will be quantified using method of moment analytical techniques (Jin et al., 1995) and 1-D multiphase transport modeling of the column experiment data. The outcome of these experiments is expected to be a set of sorption and partitioning coefficients for each of the tracers as a function of pressure, temperature, lithology, fluid saturation, HC saturation, and possibly effective surface area.

The mass-transfer mechanisms selected for testing were chosen because they parallel interactions anticipated between the injected CO_2 and subsurface phases present along the transport pathway. Thus, CO_2 will also be included with the tracer injections to determine the relative transport behavior of CO_2 and tracers under reservoir conditions. Co-injection of CO_2 and tracers will provide a means for relating isotopic fractionation to tracer partitioning at both laboratory and field scales.

The experiments are designed to progress from simple systems to more complex systems: single phase (solid), dual phase (solid, brine), dual phase (solid, HC), three phase (solid, brine, HC), and Frio core materials. Columns will be filled with solid materials (clean quartz sand, carbonate, clay, and mixed reservoir solids) and each will be used for a succession of injections. Initial helium porosimetry measurements will be taken to obtain precise values for porosity. Brine and HC saturations will be determined by repeating the He porosimetry after saturation and subtracting

from the original pore volume. At every addition of some phase to the column, porosity will be redetermined. Thus, saturations will be known to great accuracy without having to disassemble the column to measure weight differences.

On the analytical front, PDCH has been experimentally tested, and three isomers have been separated. Perfluorodimethyl-cyclobutane (PDCB) was initially considered for experimental usage, but was discarded as a first choice because the elution time is very similar to that of perfluoromethyl-cyclopentane (PMCP). Experiments are currently underway to determine detection limits of the tracers. Standards as low as 4.4×10^{-13} gm have been detected upon the gas chromatograph.

References

Hayduk, W. and H. Laudie, 1974, Prediction of diffusion coefficients of non-electrolytes in dilute aqueous solutions. Aiche J, 20, 611–615.

Jin, M., M. Delshad, D.C. McKinney, G.A. Pope, K. Sepehrnoori, C. Tilberg, and R.E. Jackson, 1994. In Toxic Substances and the Hydrologic Sciences. Am. Inst. Hydrol., Minneapolis, Minnesota, p. 131.

Sanford, W.E., R.G. Shropshire, and D.K. Solomon, 1996, Dissolved gas tracers in ground water: Simplified injection, sampling, and analysis. Water Resource. Res., 32(6), 1635–1642.

Wilke, C.R., and C.Y. Lee, 1955, Estimation of diffusion coefficients for gases and vapors. Ind. Eng. Chem., 47, 1253–1257.

Work Next Quarter

Our efforts in the next quarter will focus on four main areas:

- Continue chemical and isotopic assessment of the gases sampled on 6/20/02 at Lost Hills, California. Obtain samples during the next water-injection interval (9/02).
- Initiate high-pressure (1–100 bar) CO_2 adsorption/desorption experiments on geological materials, including the Lost Hills core.
- Initiate preliminary porosimetry and PFT flow experiments, using the Ottawa Sand.
- Initiate preliminary modeling (with Berkeley Lab) of tracer behavior determined from dynamic flow experiments.

Subtask B-3A: The Frio Pilot Test-Monitoring with Introduced Tracers and Stable Isotopes

Goals

The goal of this effort, which began this quarter, is to provide tracer and stable isotope methods that will help quantify the fate and transport of CO_2 injected into the subsurface at the Frio Formation, Texas site (Task E). The resulting data will be used to calibrate and validate predictive models used for (1) estimating CO_2 residence time, reservoir storage capacity, and storage mechanisms; (2) testing injection scenarios for process optimization; and (3) assessing the potential leakage of CO_2 from the reservoir.

Accomplishments This Quarter

- We conducted preliminary mineralogical characterization of the sandstone sample of the Frio Formation provided by BEG.
- We obtained pore-size, pore-volume, and surface-area data on the Frio sandstone sample from N_2 BET analysis.
- We obtained CO_2 adsorption/desorption isotherms for CO_2 on Frio sandstone at 23.6°C.

Progress This Quarter

Preliminary Mineralogical Evaluation of BEG Frio Sandstone Sample

A sandstone sample of the Frio Formation was obtained from BEG that purportedly is representative of the Frio horizon into which CO_2 will be injected next year. It was taken from a depth of 8185–8185.5 feet; its designation is C09013, Felix Jackson #62. Part of the sample was sent to ORNL by Larry Myer of Berkeley Lab who will be performing petrophysical tests on a core taken from a larger piece. According to Paul Knox of BEG, sand from this depth is similar to the "B" or "C" Sands in the injection test area. Standard petrographic and x-ray diffraction methods were used to characterize the sample. The sandstone is extremely friable with grains averaging between ~0.25 and 0.5 mm in diameter. Mineralogically, this sample is fairly typical of diagenetically altered Frio Formation reported in the literature by L. Land and his students. The sample is dominated by several kinds of feldspars, including plagioclase, K-feldspar, secondary albite, and quartz (detrital as well as overgrowths), with minor kaolinite, carbonate, chlorite, rock fragments (chert-replaced limestone, limestone, shale), and very rare heavy minerals (e.g., zircon). A comparison of samples treated with acid indicates a carbonate content of less than about 5%.

N_2 BET Characterization of the Frio Sandstone

A Quantachrome surface area and pore size analyzer was used to characterize a loosely disaggregated split of the Frio sandstone. Five separate measurements were made of the surface area, which averaged 1.9655 ± 0.0133 (1σ) m^2/g, much higher than we anticipated given its reasonably coarse grain size. Three different dominant pore widths were determined: 3.5–5 Å, 8–9Å, and 35–40Å. Finally, the total pore volume was determined to be 0.008514 cc/g.

CO_2 Sorption on the Frio Sandstone

CO_2 adsorption and desorption isotherms were measured for the Frio sandstone sample at 23.6°C. These results are shown in **Figure 20**, along with results we obtained on CO_2 behavior from the Lost Hills #4 sample (17°C). We have plotted these results in units of cubic feet of CO_2 per square meter of solid area versus pressure of CO_2 (up to 1 bar). Although "cubic feet" is an unconventional unit, it helps illustrate the magnitude of the sorption process in units that are used in injection testing (typically millions of cubic feet per day or MCF/D). The basic geometry of both sets of curves is similar, and they show a modest adsorption at very low pressure of CO_2, followed by a plateau or gradual increase (as in the case of the Frio sandstone) in sorption up to the maximum tested, one bar.

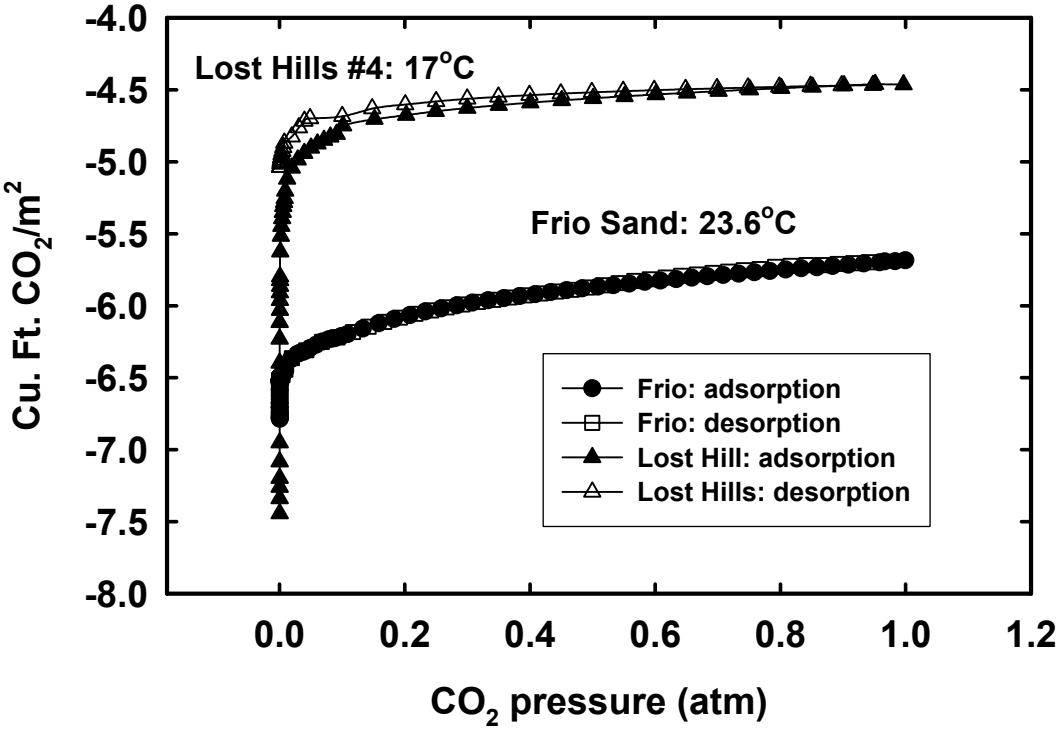

Figure 20. Adsorption-desorption isotherms for CO_2 (in cu.ft./m^2) versus CO_2 pressure at 23.6°C for the Frio sandstone sample and 17°C for the Lost Hills Sample #4.

The adsorption and desorption isotherms reflect different characteristics of a porous solid as the pressure increases from low to high pressure. In low-pressure regions, their shape is determined by the interaction between the solid surface and the adsorbate molecules. At higher pressures, the shape of the isotherms may reflect the filling of micropores and mesopores where adsorption is enhanced by the presence of closely spaced opposite walls (cooperative adsorption). In such pores, a monolayer takes up a significant fraction of the volume. If still larger pores are present, they may be then filled at still higher pressures by consecutive layers of condensing adsorbate (this is not possible if the adsorbate is a gas in its bulk phase). The mechanism of emptying the pores is (in general) different from filling; hence there is hysteresis, which is minimal for both solids (**Figure 20**). If the interaction between the solid surface and the gas molecules is stronger than the intermolecular forces in the adsorbate, the adsorbate will tend to cover the solid with a monomolecular layer at a very low pressure. This will show in the adsorption isotherm as a steep "knee" starting from zero pressure and leveling off as the monolayer is completed. This is the case for the Lost Hills sample. After the molecular-size micropores are filled, basically no more adsorption occurs, except for a small amount between particles, since it is a powder. The Frio sample has a slightly more open structure, which results in the small but steady increase in adsorption with pressure. Although most of the surface is probably comprised of micropores, the mesopores have enough volume that they too fill with CO_2 at higher pressures. Note that sorption for the Lost Hills sample is roughly one and a half orders of magnitude greater than that of the Frio sandstone, despite its surface area (1.418 m^2/g) being slightly less than that of the Frio sample. The presence of hydrocarbons in the Lost Hills sample likely plays a major role in producing this difference.

Work Next Quarter

Our efforts in the next quarter will focus on four main areas:

- Complete a 0°C adsorption/desorption experiment on the Frio sandstone sample at low pressure and initiate high-pressure CO_2 sorption experiments up to 50°C.
- Characterize the chemistry and stable isotopes of fluid, gas, and solid Frio sample obtained from the 50°C batch experiment currently in progress.
- Characterize the gas chemistry and stable isotopes of a sample provided by Jonathan Sterne of BP, taken from one of their hydrogen producing plants in Texas City, Texas. This gas will be very similar to that used in the Frio Brine Pilot Project (Task E).
- Assist in drafting the permitting documents needed for the Frio injection test.

Task C: Enhance and Compare Simulation Models

Subtask C-1: Enhancement of Numerical Simulators for Greenhouse Gas Sequestration in Deep, Unmineable Coal Seams

Goals

To improve simulation models for capacity and performance assessment of CO_2 sequestration in deep, unmineable coal seams.

Previous Main Achievements

- Reservoir simulator-code comparison studies are underway, providing a mechanism for establishing current capabilities, needs for improvement, and confidence in simulation models. Based on this comparison study, the newly improved numerical simulators—CMG's GEM, ARI's COMET3, CSIRO/TNO's SIMED II, and BP's GCOMP—have been validated.
- Comparison of the first two sets of simple numerical simulation problems in Part I with pure CO_2 injection has been completed. The results have been published in SPE paper No. 75669.
- Field data obtained from a single-well, micropilot test with pure CO_2 injection, conducted by the Alberta Research Council (ARC) at the Fenn Big Valley site, Alberta, Canada, has been released to participants (i.e., TNO, BP, CMG and ARI) for history matching (i.e., Problem Set 5). These data provide an opportunity to validate new developments in simulation models against realistic field situations.

Achievements This Quarter

- Two new participants, Imperial College and Shell (The Netherlands), have joined the reservoir simulator-code-comparison studies. The simulators used by these participants are METSIM2 and MoReS, respectively. At present, there are seven participating simulators.
- Comparison for the first two sets of simple numerical simulation problems in Part II with flue gas injection has been documented.
- Comparison of Problem Sets 3 and 4 in Part III with more complex problems is ongoing. Preliminary results from CMG's GEM, CSIRO/TNO's SIMED II, ARI's COMET3, GeoQuest's ECLIPSE, BP's GCOMP, and Imperial College's METSIM2 are being documented.

Progress This Quarter

Newly collected numerical results from Imperial College's METSIM2 for Problem Sets 1 and 2 in Part I with pure CO_2 injection have been documented. These results will be posted on the ARC Website, together with the published results from the previous participants. This Website will be continuously updated with results from late participants.

Comparison results for Problem Sets 1 and 2 in Part II with flue gas injection have been documented. Problem Set 1 is a single-well flue-gas injection/production test, and Problem Set 2 is a five-spot flue-gas injection/production process. The participating simulators are CMG's GEM, ARI's COMET3, CSIRO/TNO's SIMEDII, BP's GCOMP, and Imperial College's METSIM2. Examples of comparison results are shown in **Figures 21 and 22** for Problem Sets 1 and 2, respectively.

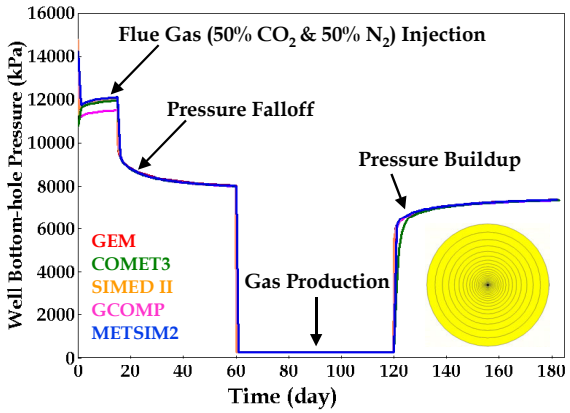

Figure 21. Problem Set 1:
Well bottom-hole pressure

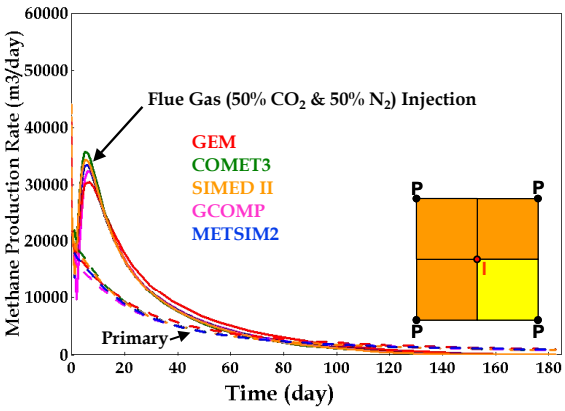

Figure 22. Problem Set 2:
CH_4 production rates

Figure 23 shows CO_2 distribution as CO_2 mole fraction in the gas phase of the fracture system for the case of a 5-spot flue-gas injection/production process (Problem Set 2).

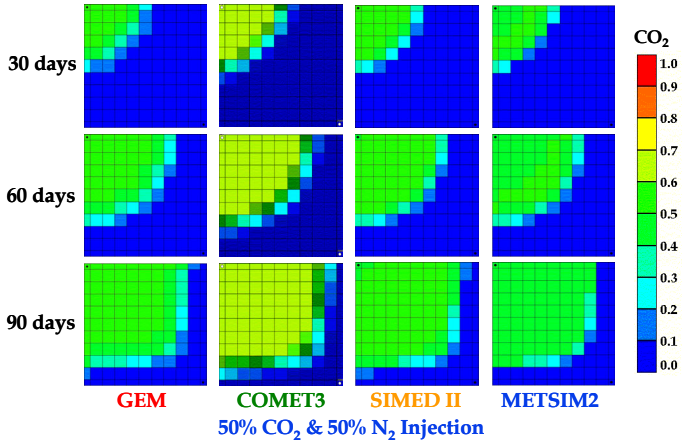

Figure 23. Problem Set 2
CO_2 Gas Mole Fraction in Coal Fracture System

Testing of the more complex Problem Sets 3 and 4 in Part III with pure CO_2 injection is ongoing: (1) Problem Set 3 is the enhancement of Problem Set 2 by taking into account the effect of gas desorption time (or gas diffusion) between the coal matrix and the natural fracture system; and (2) Problem Set 4 is the enhancement of Problem Set 2 by taking into account effect of natural fracture permeability as a function of natural fracture pressure (see **Figure 24**). Preliminary comparison results between GEM, SIMED II, GCOMP, and METSIM2 are shown in **Figure 25**.

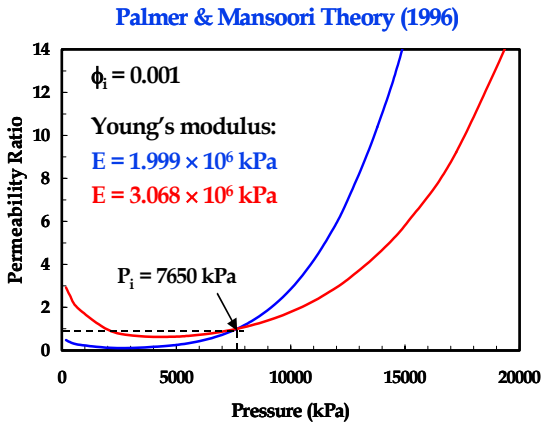

Figure 24. Problem Set 4:
Effect of Pressure Dependent Permeability

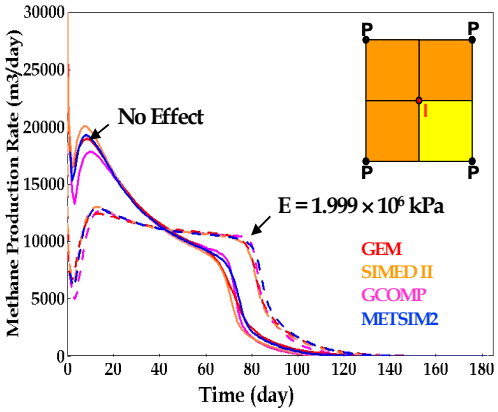

Figure 25. Problem Set 4:
CH_4 Production Rates

Work Next Quarter

ARC will collect and document numerical results from Shell's MoReS for Problem Sets 1 and 2 in Part I with pure CO_2 injection and also in Part 2 with flue gas injection. These results will be posted in the ARC Website, together with the published results from previous participants.

ARC will continue to collect and document the numerical results for Problem Sets 3 and 4 in Part III for more complex problems.

Subtask C-2: Intercomparison of Reservoir Simulation Models for Oil, Gas, and Brine Formulations

Goals

To stimulate the development of models for predicting, optimizing, and verifying CO_2 sequestration in oil, gas, and brine formations. The approach involves: (1) developing a set of benchmark problems; (2) soliciting and obtaining solutions for these problems; (3) holding workshops that involve industrial, academic, and laboratory researchers; and (4) publishing results.

Previous Main Achievements

- A first workshop on the code intercomparison project was held at Berkeley Lab on October 29–30, 2001, with the first modeling results by different groups showing reasonable agreement for most problems.

Accomplishments This Quarter

- Further simulations were performed for the intercomparison test problems.
- Additional results were obtained from participating groups.
- Comparisons of results were made, and overall satisfactory agreement was noted. Individual groups were contacted in an effort to reconcile differences.
- Write-ups for individual test problems were prepared and compiled.

Progress This Quarter

We performed further simulations for the intercomparison test problems, and received additional results from participating groups. Results from different groups were compared, agreements as well as some discrepancies were noted, and several groups were contacted in an effort to

reconcile differences. Write-ups summarizing intercomparisons were produced for individual test problems. A paper entitled "Code Intercomparison Builds Confidence in Numerical Models for Geologic Disposal of CO_2" was written and submitted to the upcoming GHGT-6 conference in Kyoto, Japan.

Work Next Quarter

Presentation materials for the intercomparison study will be prepared and presented orally at the GHGT-6 conference in Kyoto. We will make further comparisons of results from different groups, including new submissions, and will try to reconcile differences. We will begin to assemble all materials into a detailed final report on the code intercomparison project.

Task D: Improve the Methodology and Information for Capacity Assessment

Goals

To improve the methodology and information available for assessing the capacity of oil, gas, brine, and unmineable coal formations; and to provide realistic and quantitative data for construction of computer simulations that will provide more reliable sequestration-capacity estimates.

Previous Main Achievements

- A new definition of formation capacity, incorporating intrinsic rock capacity, geometric capacity, formation heterogeneity, and rock porosity, was developed for use in assessing sequestration capacity.
- An assessment of California's CO_2 sequestration capacity was carried out.
- Factors affecting the sequestration capacity of the Frio formation in Texas have been evaluated.
- The Texas Gulf Coast was targeted as an area from which a realistic data set could be generated for use in simulating brine-formation capacity.
- Location and identifying information were compiled for large industrial CO_2 emitters, and geologic data for the Frio and Oakville reservoirs were compiled.
- A realistic scenario for CO_2 injection into a brine formation was then designed for a site near Baytown, Texas; its brine-formation capacity for CO_2 storage was assessed, based on numerical-simulation studies.

Accomplishments This Quarter

Our studies showed that the contribution of residual saturation to sequestration of CO_2 was more significant than previously estimated.

We also conducted modeling studies of the Frio Brine Pilot Project CO_2 injection experiment (Task E), using a heterogeneous model of the South Liberty site, focusing on:

- The C Sand
- The impact of drilling a new injection well
- Shorter CO_2 injection periods using higher injection rates
- Addition of tracer during CO_2 injection
- Well testing prior to CO_2 injection

Progress This Quarter

Residual saturation is the fraction of an immiscible fluid that cannot be drained from a two-phase mixture in a porous medium, as a result of capillary forces in the pores. For the case of CO_2 injected into a brine formation and not into a structural or stratigraphic trap, residual saturation will strongly influence the plume geometry and sequestration effectiveness. Rock-fabric-specific information is needed to quantify residual saturation. Most of the data for the Frio Formation is

from South Texas, which is petrographically and depositionally distinct from the Houston area because of its more volcanogenic source area and a different depositional system.

We are using the core from Well Felix Jackson #62 as an example of the Frio Formation in the Houston area. We received a donation of significant amount of well data from the current field operator (i.e., five-foot logs, 125 routine porosities and permeabilities from plugs taken from whole core, 18 porosities and permeabilities from side wall plugs, five residual gas saturation measurements, 13 directional permeability measurements, and 16 grain size and mineralogy data) We are logging this core to identify depositional facies, and the entire integrated data set will provide better rock-specific petrophysics to be input into simulations.

We have developed a methodology for creating a statistically based geologic model for the pathways that would be occupied by CO_2 from a location in the upper Texas coast. This will involve extraction of data from existing compilations to create ranges of relevant data, such as closure in structural traps and height of oil and gas columns trapped against faults.

New modeling studies of the South Liberty Field, the location of the Frio pilot CO_2 injection experiment, were performed during this period. Earlier pilot-site modeling studies were described in the two previous quarterly reports. Initial studies considered CO_2 injection into the B Sand, but at the early July meeting at BEG it was decided to focus on the underlying C Sand, because it is identifiable in surface seismic data. The 12 m thick C Sand is at about 1,500 m depth.

Model Construction

Construction of the B Sand model was described in the last quarterly report; Table 1 summarizes the material properties of the model. **Figure 26** shows the TOUGH2 model of the C Sand, which contains three depositional settings. The top frame shows the entire model, with a distributary channel present at the top. The middle frame shows the model with the distributary channel removed, exposing the middle shale layer. The bottom frame depicts the model with the shale layer removed, showing the lower sand. Within each depositional setting, three facies are arranged stochastically, using the TproGS software. Each depositional setting is discretized into several model layers. In the lower sand, there is an upward-coarsening trend, with permeability and porosity increasing from layer to layer. Note that the middle shale is only 0.3 m thick. Lateral gridblock spacing is finer around the injection and monitoring wells. Each layer is rotated 15^o about the x-axis, to represent a dipping formation. Although field data suggest that the actual dip varies spatially, 15^o is considered the best average value to use. Table 1 shows the permeabilities and porosities used in the C Sand model. The characteristic curves used in the modeling studies are not site specific to the Frio, but are generic sand/shale curves that have an irreducible liquid saturation $S_{lr} = 0.3$, as well as an irreducible gas saturation $S_{gr} = 0.05$.

The top and bottom boundaries of the model are closed, to represent continuous sealing shale layers. Three of the four lateral boundaries of the model (NE, NW, SE) are closed, to represent vertical faults. In the SW direction, the model actually extends much farther than shown (y = 9,000 m), to represent an incompletely sealed fault block.

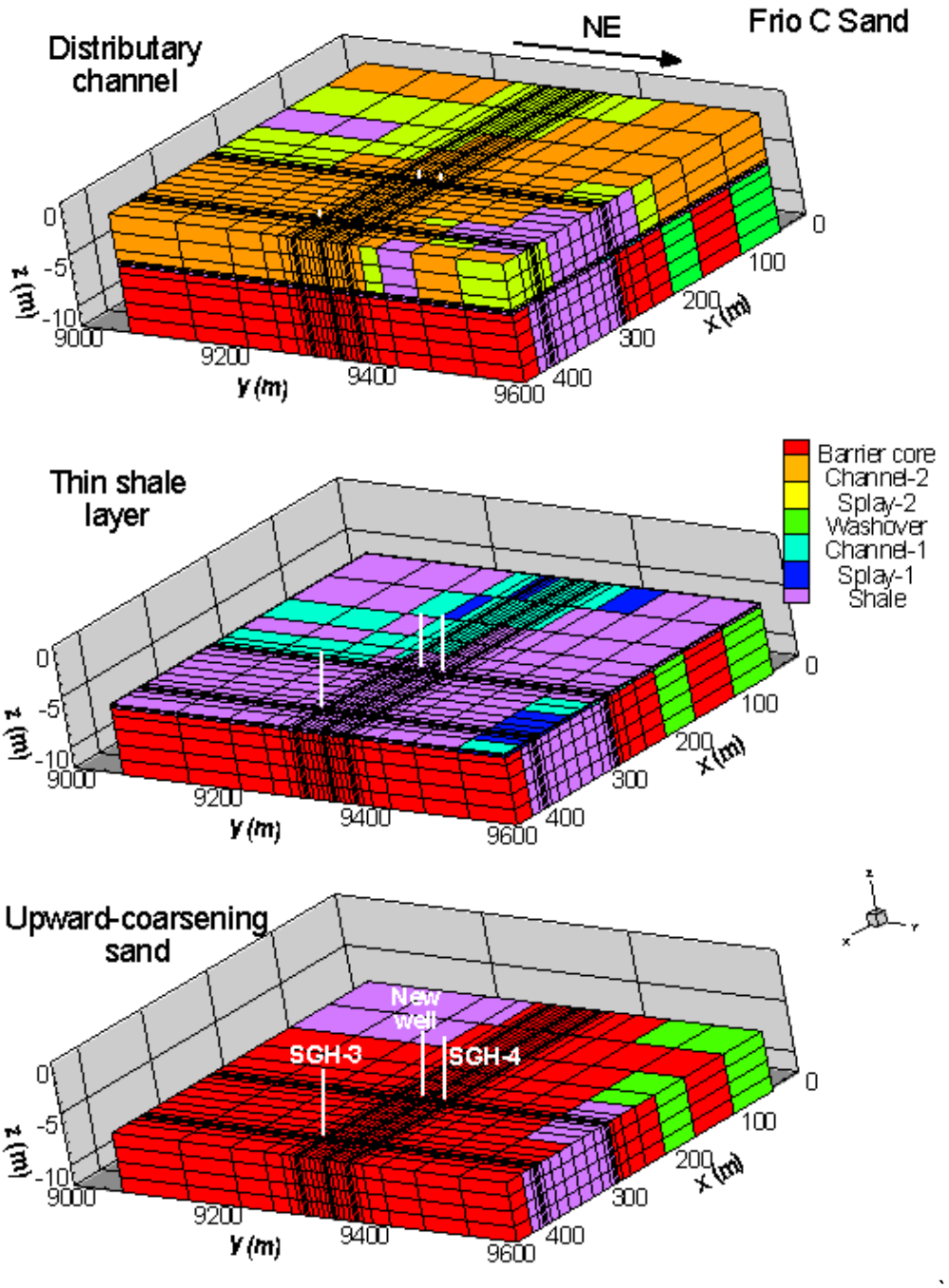

Figure 26. The TOUGH2 model of the Frio C Sand at the South Liberty field site. SGH-3 and SGH-4 are existing wells. The location labeled “new well” is the proposed location for a new injection well.

Table 1. The model permeabilities and the porosities for the various facies in the B and C Sands

B Sand						
Model layers (top to bottom)	Depositional setting (facies)	Thick-ness (m)	Horizontal permeability (md) (framework facies in bold)			Porosity of framework facies (%)
			Channel or Bar	Splay or Washover	Shale	
1-5	Upper thick sand (bar, washover, shale)	6	**700**	200	0.001	32
6-7	Middle Shale (channel, splay, shale)	3	100	30	**0.001**	10
8-9	Lower Shale (channel, splay, shale)	6	400	150	**0.001**	10

C Sand						
Model layers (top to bottom)	Depositional setting (facies)	Thick-ness (m)	Horizontal permeability (md) (framework facies in bold)			Porosity of framework facies (%)
			Channel or Bar	Splay or Washover	Shale	
1-4	Distributary channel (channel, splay, shale)	5.5	**500**	375	0.001	28
5-6	Shale (channel, splay, shale)	0.3	200	150	**0.001**	10
7-8	Upward-coarsening sand (bar, washover, shale)	1.5	**600**	450	0.001	28
9		1.5	**400**	300	0.001	25
10		1.5	**200**	150	0.001	23
11		1.5	**100**	75	0.001	20

CO_2 Injection Scenarios

As plans for the pilot test have developed, the model has evolved. Previous CO_2 injection simulations injected 5,000–7,500 tonnes over an injection period of 100 days (50–75 T/day). Operational field-work considerations make a shorter test much more practical, so injection periods of 20, 30, or 60 days are used for the current studies. Based on experience elsewhere in the Frio, the higher injection rates (up to 250 T/day) necessary to inject a given amount of CO_2 in a shorter time period should not be a problem.

The original pilot test plan used two existing wells, SGH-3 and SGH-4, as injection and monitoring wells, respectively. This configuration required large amounts of CO_2 to be injected to make breakthrough at the monitoring well likely, because the wells are about 150 m apart. Therefore, the possibility of drilling a new well is being evaluated. The new well would be an injection well and would be located about 30 m down-dip from Well SGH-4 (see **Figure 26**). With this configuration, it is expected that CO_2 breakthrough at the monitoring well can be achieved sooner and with a significantly smaller volume of injected CO_2.

Simulation Results

Table 2 summarizes the recent CO_2 injection simulations for the B and C Sands. Selected C Sand results are shown below. A more complete set of results is posted on the Reservoir Website maintained by BEG (http://inet2.beg.utexas.edu/).

Table 2. Summary of CO_2 injection simulations for the B and C Sands

B Sand						
Case	Model	Injection scenario	Injection well	Injection interval	CO_2 arrival at SGH-4 (days)	ΔP_{max} (bars)
1A	15^o dip, sides partly sealed	7,500 T/60 days (125 T/d)	SGH-3	Upper sand	53	9.9
1B		7,500 T/30 days (250 T/d)			31	14.9
2A	30^o dip, sides partly sealed	7,500 T/60 days (125 T/d)			47	10
2B		7,500 T/30 days (250 T/d)			28	15
5A	15^o dip, sides all sealed	7,500 T/60 days (125 T/d)			54	18
5B		7,500 T/30 days (250 T/d)			32	21
O1A	15^o dip, sides all open	7,500 T/60 days (125 T/d)			60	3.9
O1B		7,500 T/30 days (250 T/d)			41	7.4

C Sand						
Case	Model	Injection scenario	Injection well	Injection interval	CO_2 arrival at SGH-4 (days)	ΔP_{max} (bars)
C3A	15^o dip, sides partly sealed	7,500 T/60 days (125 T/d)	SGH-3	Whole	None	10.7
C3B		7,500 T/30 days (250 T/d)			None	13.7
C4A		7,500 T/60 days (125 T/d)	New well	Upper sand	3.6	10.7
C4B		7,500 T/30 days (250 T/d)			1.9	15.4
C5B		5,000 T/20 days (250 T/d)		Lower sand	1.3	15.0
C6B				Whole	3.0	11.3

Figure 27 shows pressure and CO_2 in the gas and aqueous phases as a function of time for the locations of the injection well (the proposed new well) and two monitoring wells (SGH-3 and SGH-4) for Case C5B. Injection occurs over the entire lower sand thickness; the results shown correspond to the top of the lower sand. The gas- and liquid-phase CO_2 quantities shown represent the volume fractions of the pore space occupied by CO_2 in a supercritical gas-like phase (C_g) and by CO_2 dissolved in the aqueous phase (C_l). The leading edge of the CO_2 plume arrives at Well SGH-4 after 1.3 days of injection, and the trailing edge passes the well after about 230 days. The plume does not reach well SGH-3.

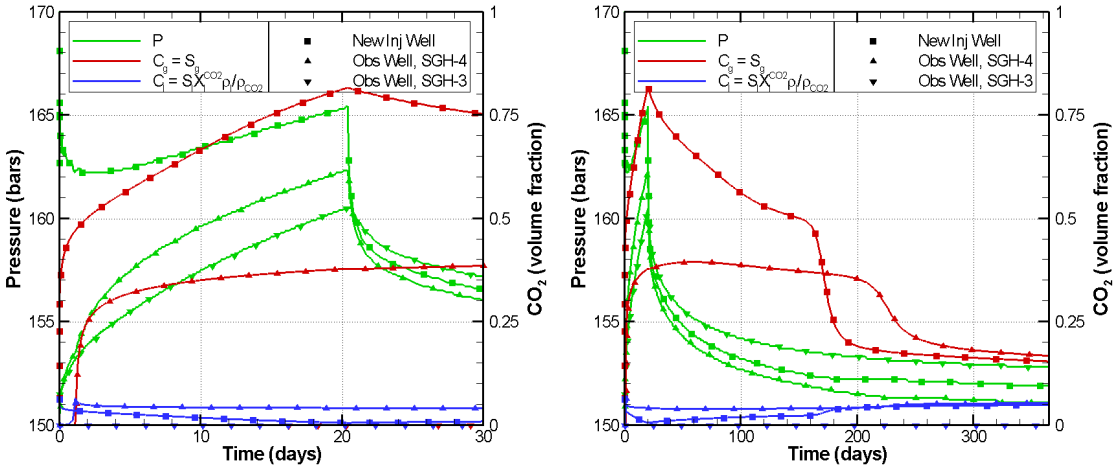

Figure 27. Modeled pressure and CO_2 at well locations for Case C5B. The frame on the left corresponds to the 20-day injection period and the first 10 days of the rest period; the frame on the right, the entire one-year simulation period.

Spatial distributions of the CO_2 are shown in **Figures 28** through **30** for Case C5B. The top view **(Figure 28**) illustrates how the CO_2 plume gradually moves updip under the influence of buoyancy flow after injection ends. The residual gas saturation S_{gr} = 0.05 is apparent around the injection well after one year. The side view (**Figure 29**) shows how the upward-coarsening nature of the lower sand channel acts in concert with buoyancy flow to greatly enhance flow into the upper portion of the lower sand channel.

Figure 30 gives a side view through x = 200 m, where gaps in the thin shale layer exist (see **Figure 26**), allowing the injected CO_2 to migrate upward. Plots show both gas-phase and liquid-phase (dissolved) CO_2. A logarithmic color scale is used to enable showing both phase distributions with the same scale. At later times, comparable amounts of CO_2 are found in each phase.

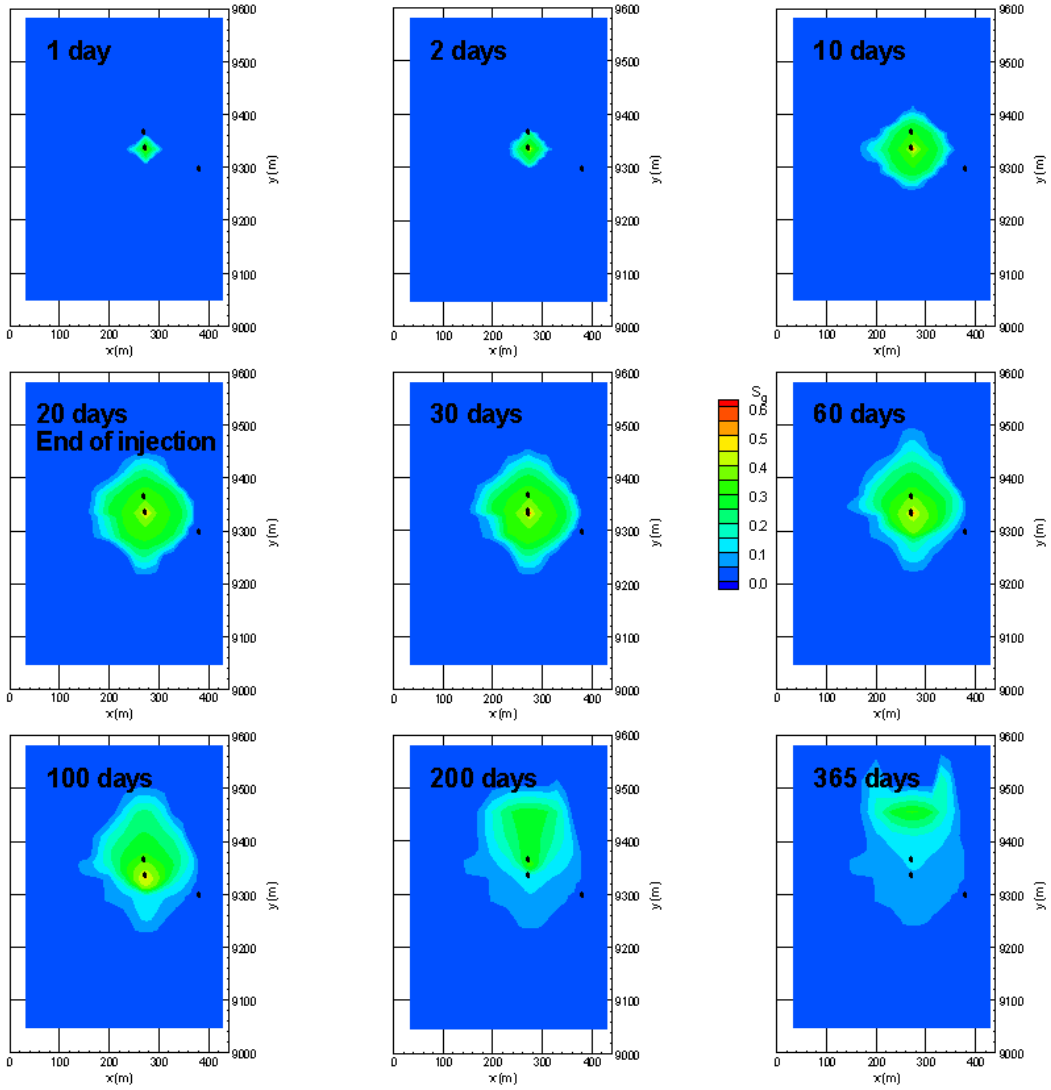

Figure 28. Modeled gas-phase CO_2 distributions at the top of the lower sand during and after the 20-day injection period for Case C5B

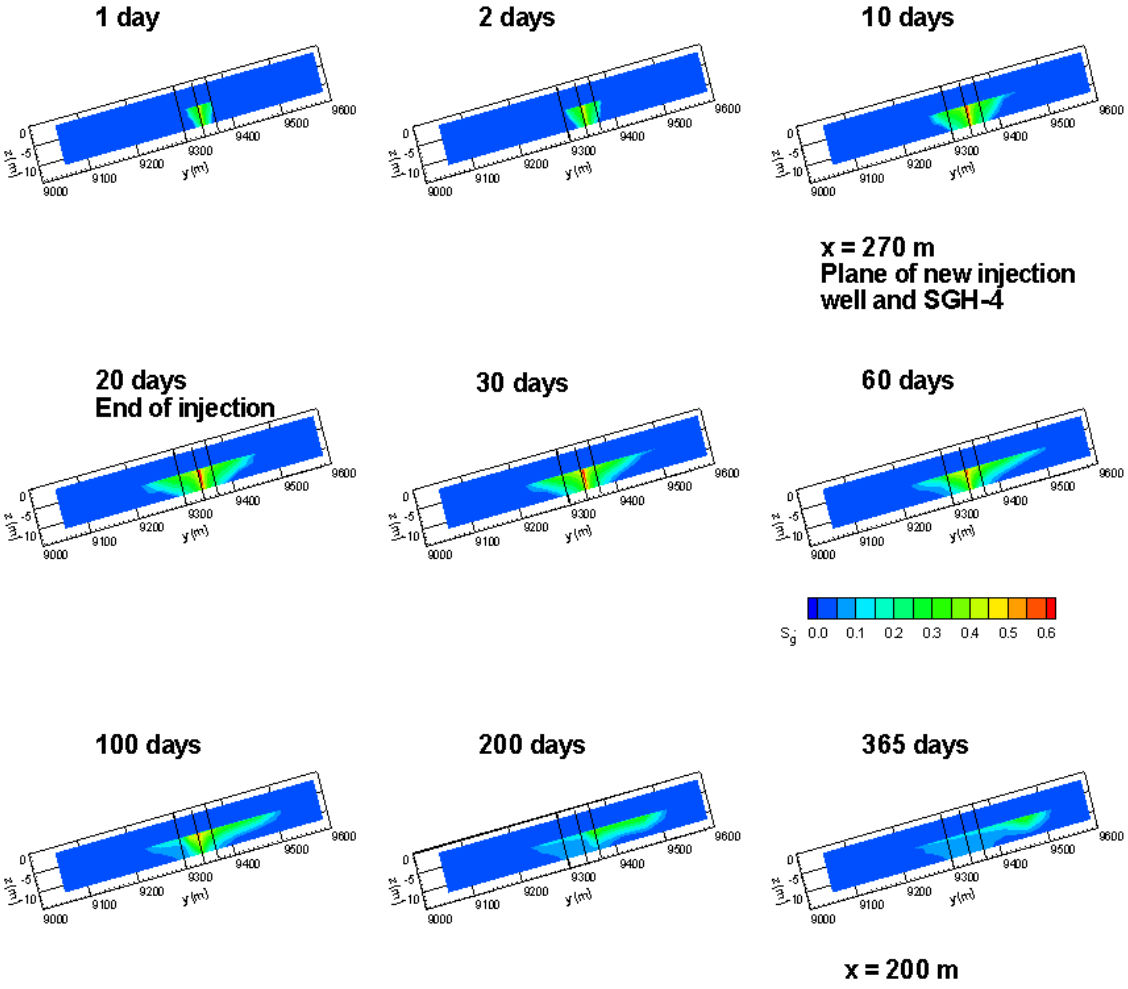

Figure 29. Modeled gas-phase CO_2 distributions in a vertical section along well SGH-4 and the proposed new injection well, during and after the 20-day injection period for Case C5B. The three black lines identify the y-coordinates of (from left to right), well SGH-3, the proposed new injection well, and well SGH-4.

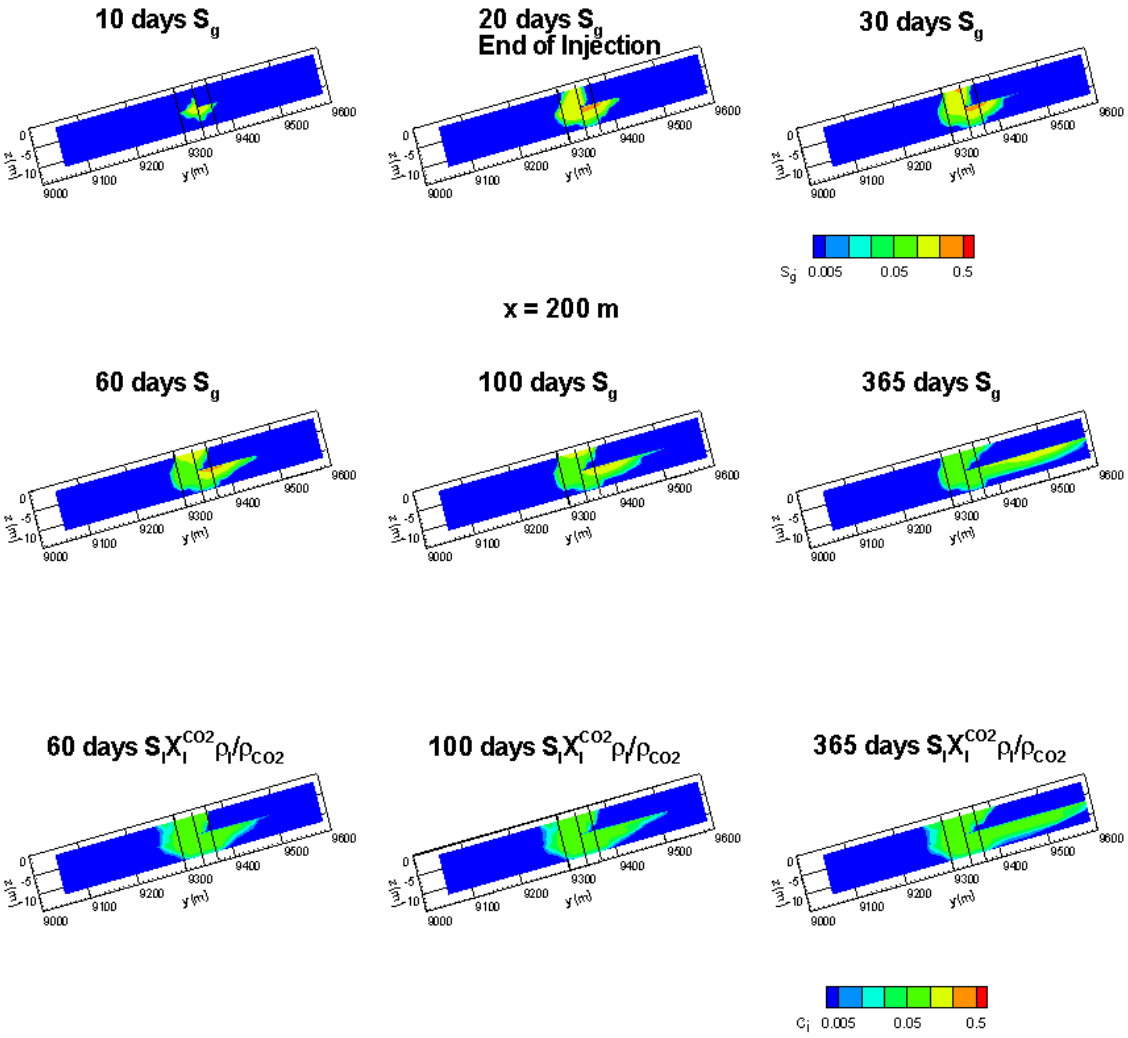

Figure 30. Modeled CO_2 distributions in a vertical section at x = 200 m, where gaps in the shale layer exist, during and after the 20-day injection period for Case C5B. $C_g = S_g$ and $C_l = S_l X_l^{CO2} \rho_l / \rho_{CO2}$ are plotted using the same color scale.

Figure 31 shows the distribution of pressure change at the top of the lower sand at the end of the 20-day injection period for Case C5B. The maximum pressure increase caused by CO_2 injection is 15 bars, but this change is localized around the injection well. Over most of the model, the pressure increase is about 10 bars. The two regions with almost no pressure increase correspond to the locations of shale lenses within the lower sand (**Figure 26**). Shale permeability is so low that the pressure response to injection does not propagate into the lenses. Consequently, the flow field bypasses them (e.g., see the final frame of **Figure 28**).

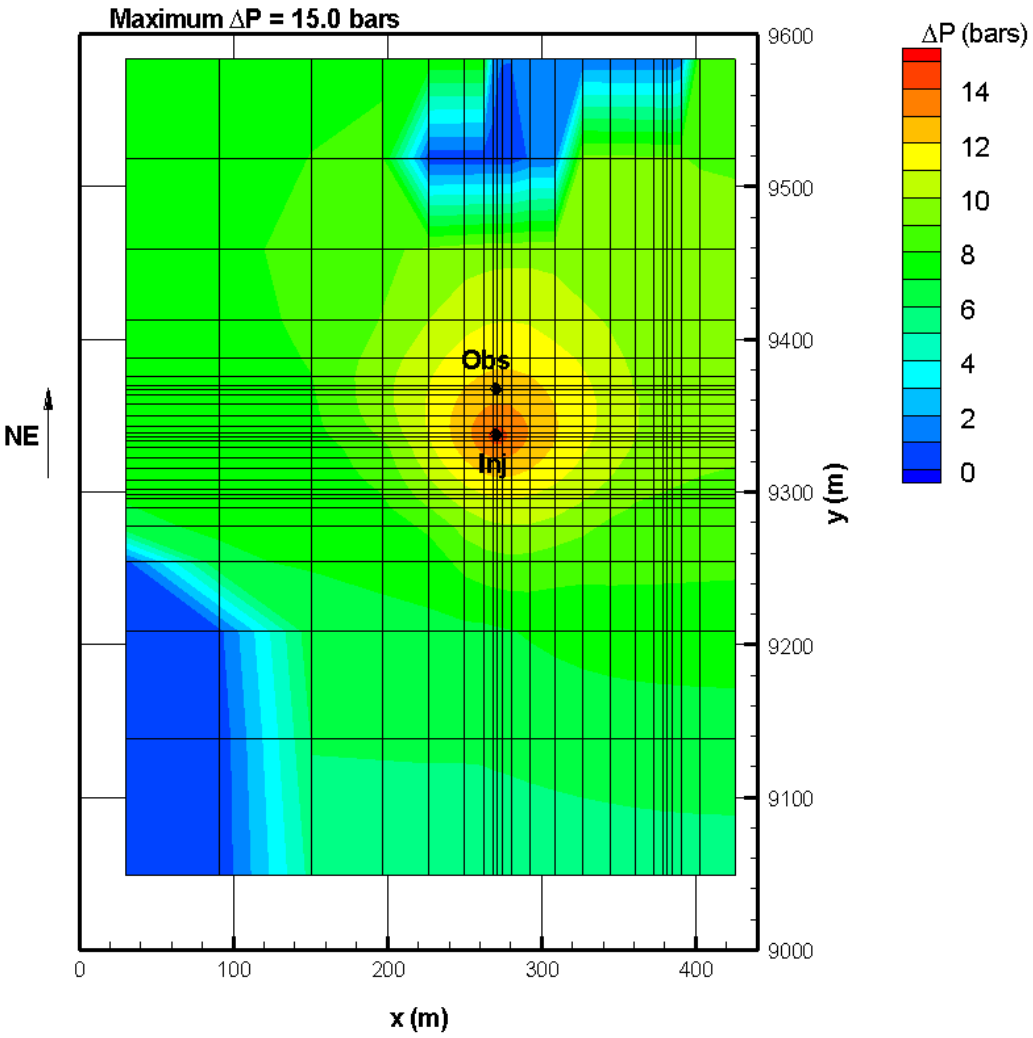

Figure 31. Pressure increase at top of the lower sand at the end of the injection period for Case C5B

For the B Sand simulations, the lateral boundary conditions (see Table 2) have a strong effect on the pressure response, as shown in **Figure 32**. Because all of the C Sand simulations use the same lateral boundary conditions, the main factor affecting the pressure response is the injection rate per unit thickness. For example, the pressure increase is larger for Cases C4B and C5B than for Cases C3B and C6B: the injection interval is only one-half the sand thickness in the former cases, but is the entire sand thickness in the latter cases.

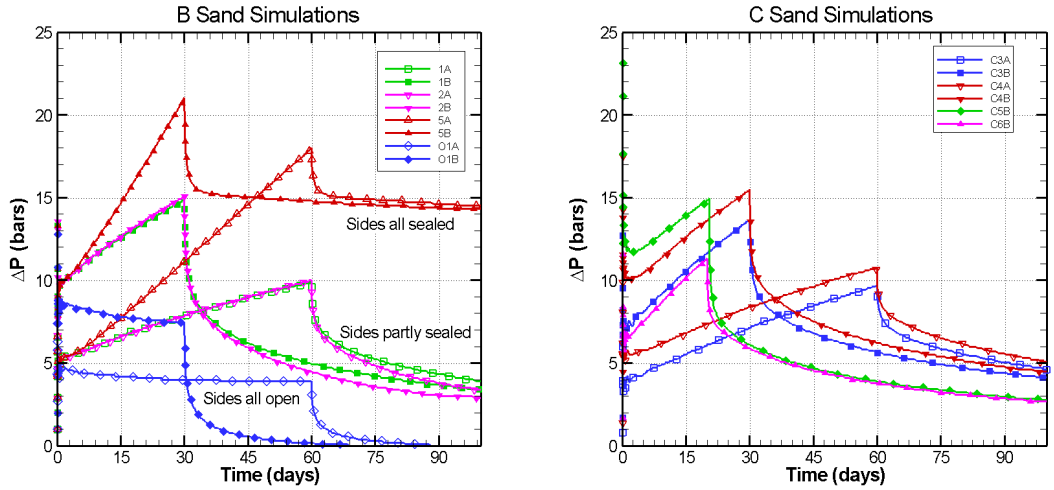

Figure 32. Pressure response at the top of the injection interval for the various B and C Sand cases

Figure 33 shows CO_2 breakthrough curves at Well SGH-4 for the various B and C Sand cases. All the B Sand cases use Well SGH-3 as the injector. Breakthrough time is shorter for Case 2B (30° dip) because buoyancy flow is stronger than for the other cases. Breakthrough time is longer for Case O1B (open lateral boundary conditions) because the CO_2 plume spreads in all directions from the injection well, rather than being focused toward the monitoring well by sealing faults. Breakthrough time is slightly longer for Case 5B (completely sealed fault block) than for Case 1B (partly sealed fault block) because the higher pressures arising for Case 5B (**Figure 32**) create a denser, more compact CO_2 plume. For the C Sand case using Well SGH-3 as the injection well, breakthrough at Well SGH-4 never occurs. This is because the entire C Sand thickness is used as the injection interval (~12 m) compared to the thinner injection interval for the B Sand (6 m). Thus, the thicker plume does not extend far enough laterally to reach well SGH-4. In all cases, injecting at a higher rate for a shorter time period produces a shorter breakthrough time (Case 1A compared to 1B, Case 2A compared to 2B, etc.)

Breakthrough times are significantly shorter for the C Sand simulations that use the proposed new injection well. Case C6B has a longer breakthrough time because the injection interval extends over the entire 12 m sand thickness. Case 5B has a shorter breakthrough time because injection is concentrated in the upper portion of the lower sand (see **Figure 29**).

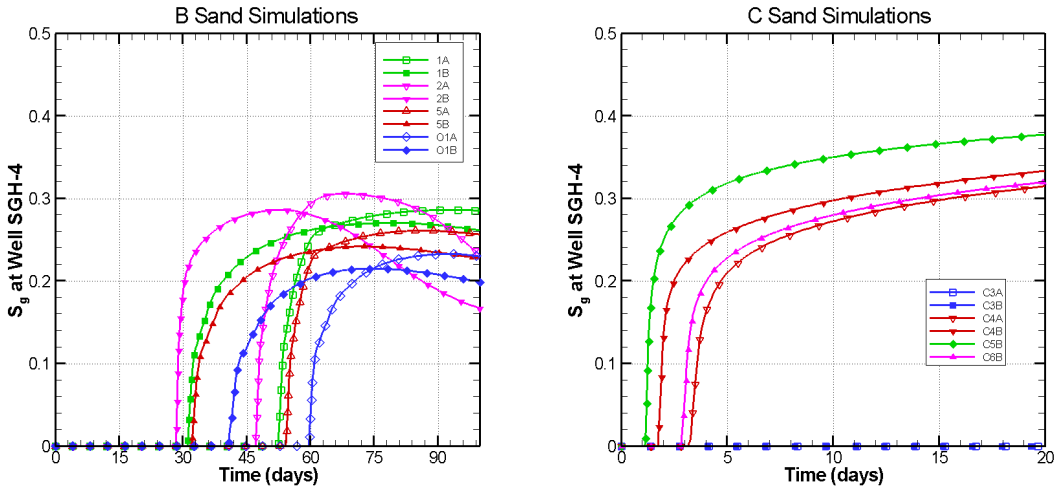

Figure 33. CO_2 breakthrough curves for various B and C Sand cases

Other Simulations

Prior to CO_2 injection at the South Liberty site, interference well tests are planned for site characterization purposes. Preliminary simulations of well tests were carried out to begin the process of designing them and to optimize sensitivity to major points of uncertainty in the geologic and hydrologic models. Key questions include the nature of the lateral boundary conditions (whether faults are open or closed) and *in situ* phase composition (whether the fluid in the formation is liquid brine, brine with dissolved gas that comes out of solution when pressure decreases, or brine with immobile gas).

Injecting tracers along with CO_2 are being considered as part of the pilot test. A modified version of TOUGH2 was developed, to allow modeling of a tracer that partitions between the gas and aqueous phases, along with supercritical CO_2, water, and salt. Two preliminary simulations using a noble gas tracer (argon) were done. A key feature of noble gas tracers is that they remain primarily in the gas phase, whereas a significant amount of CO_2 dissolves into the aqueous phase. Thus, when CO_2 and argon (Ar) are injected together, the Ar front moves ahead of the CO_2 front, akin to chromatographic separation. The amount the Ar front moves ahead of the CO_2 front provides information on the amount of CO_2 dissolving in the aqueous phase, which in turn provides information on the nature of the interface between the liquid and gas phases. The phase interface is a fundamental property of two-phase flow systems and cannot be investigated solely in laboratory studies, because the field-scale heterogeneity of real systems has a strong influence on it.

The first tracer simulation considers CO_2 and Ar injection into a homogeneous 1-D radial model with fine grid resolution; the second uses the 3-D model of the B Sand. **Figure 34** shows profiles for the radial model, illustrating the concept. The gas saturation (S_g) profile identifies the CO_2 plume. The Ar profile shows a spike just beyond the leading edge of the CO_2 plume, which is the chromatographic signature. **Figure 35** presents CO_2 and Ar distributions obtained with the B Sand model. The picture is harder to interpret, because the flow processes are complicated by the addition of buoyancy flow and geologic heterogeneity, and because the grid is relatively coarse. The plots showing the lower region of the injected plume (z = –5m) show the expected spike of Ar just beyond the perimeter of the CO_2 plume, but the plots showing the upper region (z = 0) do not. This and other tracer issues will be further investigated in the coming months.

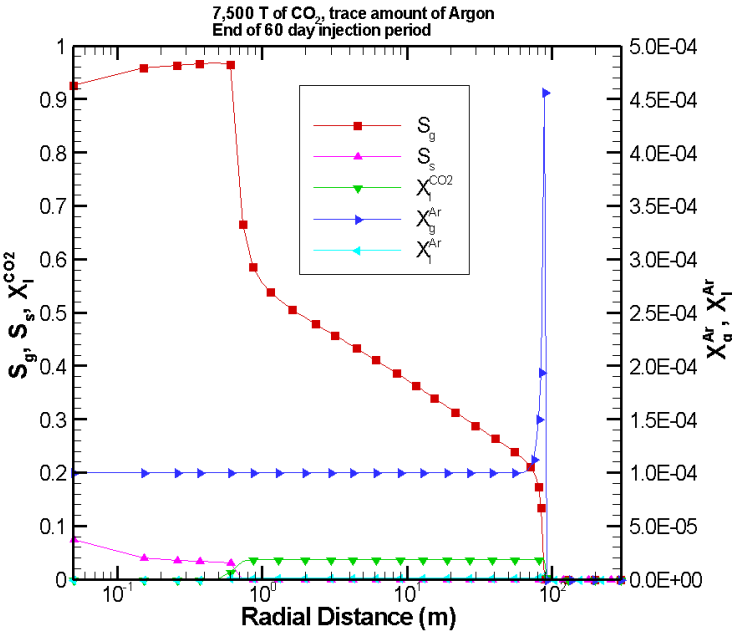

Figure 34. Profiles at the end of a 60-day injection period of CO_2 and Ar, using a –D radial model. S_g is gas (primarily CO_2) saturation, S_s is precipitated salt saturation, X_l^{CO2} is the mass fraction of CO_2 dissolved in the aqueous phase, and A_g^{ar} and L_a^{rs} are the mass fractions of argon in the gas and liquid phases, respectively.

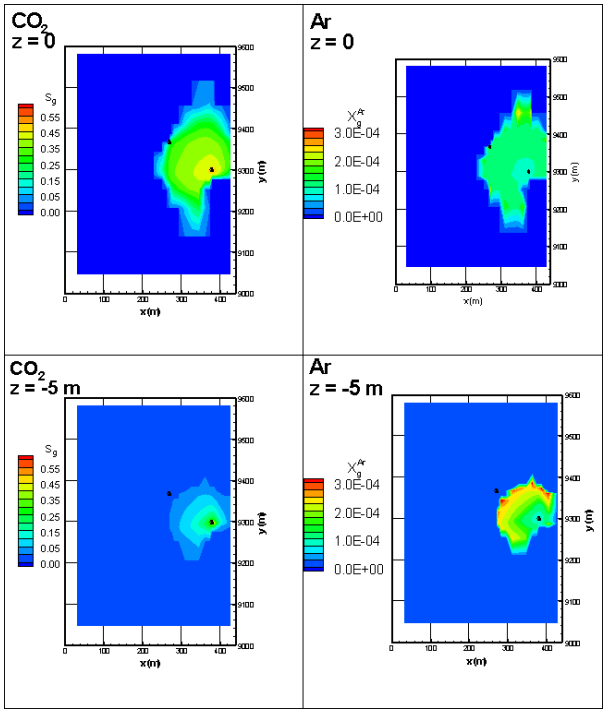

Figure 35. Distribution of CO_2 and Ar at the end of a 60-day injection period, using the B Sand model

Conclusions

Injection into the C Sand rather than the B Sand does not change the behavior of the CO_2 plume dramatically, since the two sands have similar properties, depth, and thickness. In contrast, using a new injection well instead of well SGH-3 has two significant benefits: (1) breakthrough of CO_2 at the monitoring well occurs much sooner, enabling a much shorter injection period; and (2) much less CO_2 needs to be injected. Both these changes reduce the cost and simplify the logistics of the pilot test. Additionally, using a new well for injection improves the reliability and safety of the injection process. The addition of a tracer-modeling capability to the CO_2/brine version of TOUGH2 enables study of a potentially powerful tracer technique for investigating two-phase flow processes accompanying CO_2 sequestration.

Work Next Quarter

Further simulations will replicate more closely the currently envisioned pilot-site test conditions:

- We have ordered detailed commercial Geomap structural maps for the Houston area and will compile statistics to describe typical volumes within fault closure and quantify the pathways of spillover from the structures. These data will be used to develop a statistically based geologic model for the pathways that would be occupied by a large plume of CO2 during the injection and post injection phase of sequestration, to assess the trapping and sequestration effectiveness.
- Characteristic curves (relative permeability and capillary pressure as a function of phase saturation) based on Frio petroleum-reservoir data will be incorporated into the TOUGH2 simulations. Thus far, generic sand/shale characteristic curves have been used. Moreover, the applicability of characteristic curves developed for oil-water or water-air systems to supercritical-CO2/brine systems has not been fully established. Laboratory studies being conducted elsewhere within the GEO-SEQ project should help address this issue. However, field-scale measurements are also necessary, because multiphase flow effects and geologic heterogeneity can produce coupled results that cannot be reproduced in the laboratory. If two-phase conditions are encountered during the site characterization well-testing activities to be conducted prior to CO2 injection, analysis of the resulting pressure transients may enable features of the characteristic curves to be inferred. Pressure-transient monitoring during CO2 injection itself will also be useful in this regard.
- The South Liberty geologic model developed at BEG is currently being adapted to work with TOUGH2. When this work is complete, TOUGH2 simulations will switch from the present “Version 0” model to a “Version 1” model that incorporates far more detailed geological information. For example, in the Version 0 model, the Frio B and C Sands are modeled as planar layers with a uniform dip, which are separated by an impermeable shale layer. Lateral fault-block boundaries seal perfectly. In the Version 1 model, sand layers are not planar and have slopes that vary in two directions. Even more importantly, intra-fault-block faults offset the sands significantly, potentially enabling communication among all three (A, B, and C) Frio sands included in the model.
- Further studies on the design of the interference tests and the addition of noble-gas tracers to injected CO_2 will be carried out.

Task E: Frio Brine Pilot Project

Goals

To perform numerical simulations and conduct field experiments at the Frio Brine Pilot site, near Houston, Texas, that:

- Demonstrate that CO_2 can be injected into a saline formation without adverse health, safety, or environmental effects.
- Determine the subsurface location and distribution of the cloud of injected CO_2.
- Demonstrate understanding of conceptual models.

- Develop the experience necessary for the success of large-scale CO_2 injection experiments.

Note: This task does not include work being done by the Texas Bureau of Economic Geology under the project "Optimal Geological Environments for Carbon Dioxide Disposal in Brine Formations (Saline Aquifers) in the United States," funded under a separate contract.

Accomplishments This Quarter

- We developed a time line and a more detailed plan for implementation of modeling and monitoring techniques at the brine-sequestration pilot test.
- We designed experiment options that could be done if drilling a new and more closely spaced injection well effectively substitutes for a recompleted oil production well originally considered for the project.

Progress This Quarter

A planning workshop was held July 8–9 at BEG (Austin, Texas) to explore the interrelationships among the modeling and monitoring techniques proposed by the GEO-SEQ team for conducting the Frio Brine Pilot Test. We plan to move toward in fielding these techniques at the site. The meeting provided in-depth information exchange among the GEO-SEQ Task E team, BEG staff charged with site characterization, the field service provider (Sandia Technologies), EOR engineer Bill Flanders and contributor BP, and the permitting agency, the Texas Commission on Environmental Quality. Decisions were reached to inject into the "C Sand" and to recommend drilling a new injection well. A detailed time line was prepared to document the sequence of tests, and interactions between tests were examined and conflicts resolved.

A proposal that substitutes construction of a new injection well for the retrofitting of a 50-year-old oil well was prepared. The new well would be closer to the monitoring well and directly down dip, and therefore require less CO_2 and a shorter injection period. GEO-SEQ contributions to this proposal centered on the additional research that could be conducted if a new well were drilled. This may include open-hole logging, coring the injection interval and seals, installation of tubing-conveyed geophones to facilitate seismic data collection during injection, essentially continuous downhole pressure and temperature measurement, and special core analysis to provide laboratory-based data. These data would be used for comparison with observed downhole residual-saturation behavior of the injected CO_2 plume.

Work Next Quarter

Activities will focus on preparing the report to support the Class 5 permit application to Texas Commission on Environmental Quality and the NEPA EA. The GEO-SEQ contributions to these tasks will include modeling of the pressures and area of elevated pressure, modeling to support assessment of the long-term fate of CO_2, chemical analysis of the CO_2 to be injected, and other input as required.

We will work with stakeholders in the Houston area to prepare for public hearings to be held on these documents in the future.